UNIVERSITÀ DEGLI STUDI DI PADOVA

Dipartimento di Fisica e Astronomia "Galileo Galilei"

Master Degree in Physics

Final Dissertation

Reynolds stress dynamics and turbulent energy transfer during stimulated H-Mode transition in RFX-mod tokamak

Thesis supervisor

Prof. Emilio Martines

Thesis co-supervisor

Dr. Nicola Vianello

Candidate

Samuel Bresciani

Academic Year 2019/2020

"We can not solve our problems with the same level of thinking that created them."

Albert Einstein

UNIVERSITÀ DEGLI STUDI DI PADOVA

Abstract

Physics

Dipartimento di Fisica e Astronomia "Galileo Galilei"

Master Degree

Reynolds stress dynamics and turbulent energy transfer during stimulated H-Mode transition in RFX-mod tokamak

by Samuel BRESCIANI

The present thesis has been devoted to the investigation of the turbulence properties in the edge region of RFX-mod operated as a tokamak during the transition from Low confinement (L-mode) to High confinement (H-mode) mode aided by the use of a biasing electrode inserted into the plasma. The mechanism of L-H transition is not fully understood in the framework of thermonuclear plasma science. Among the hypothesis, it has been suggested that turbulence itself may contributed to the formation of the sheared $\mathbf{E} \times \mathbf{B}$ flow in the external region which represents a distinct feature of the H-Mode. The proposed model foresees a transfer of momentum from fluctuations to the mean plasma flow through the Reynolds stress mechanism. This has been observed in various devices but no detailed analysis has been done so far on L-H transition induced by the application of an electrode capable of providing additional radial electric field and thus $\mathbf{E} \times \mathbf{B}$ flow. The thesis has been done on RFX-mod, run as a tokamak in Upper Single Null (USN) configuration, and the analysis has focused on data of the external region, close to the separatrix by means of an insertable probe. The Reynold stress contribution to the transition from L to H mode have been determined with its relation to the increase of flow velocity. A robust change is seen in velocity shear across the transition. An analysis of the dynamics of the flow is presented reporting that additive terms to the model have to be considered for a complete description of the phenomenon in case of induced biased H-Mode and some theoretical hypothesis have been proposed in accordance with experimental results. Eventually contribute of turbulences to viscosity and diffusive momentum have been studied confirming the results previously obtained in the thesis.

To my family...

Summary

This thesis is devoted to the investigation of plasma turbulence in the periphery of a tokamak device during the transition from a low confinement to an improved confinement regime. With this transition at the edge of the plasma steeper pressure and temperature gradients are observed with the creation of an external transport barrier. This occurs with the increase of radial electric field and hence the $E \times B$ flow velocity with its shear. The dynamics of this flow can be modelled through the Zonal Flow theory but at present is not completely understood. This model suggests an increase in the flow velocity through the action of the Reynolds stress which combines the contribution of velocity fluctuations along orthogonal directions. It can be seen also perturbing the momentum balance equation as reported in this thesis.
The H-Mode has been discovered the first time thanks to the exceeding of a threshold from the heating power necessary to warm the plasma. Different methods have also being explored, among which the direct increase of the radial electric field in the external region through the exploitation of an insertable electrode which is biased with respect to the vacuum vessel. This is the method used on RFX-mod which allowed the transition from Low Confinement (L-Mode) to High Confinement (H-mode) in a controlled way. The properties of the flow are studied thanks the employment of Langmuir probes. The discharges analysed in the present thesis have been run in Upper Single Null configuration with Deuterium gas. In this thesis has been found that in the original Zonal Flow model other forces has to be considered to describe correctly the $E \times B$ flow in the case of biased induced H-Mode.

Chapter 1 An introduction to features of plasma physics is presented from a theoretical and experimental point of view with focus on tokamak configuration of interest for this thesis.
Chapter 2 The properties that define the High confinement Mode are reported. The Zonal Flow theory that regulates the $E \times B$ flow acceleration is presented with the importance of the Reynolds stress in increasing the velocity and hence reducing the turbulences. A mention to the theoretical reasons of the Reynolds stress is done too.
Chapter 3 The measurement system is reported with the features of a Langmuir probe. The biasing electrode functioning is reported too. Eventually the properties of the discharges analysed are illustrated.

Chapter 4 The experimental analysis starts from the characterisation of the obtained H-Mode through the changes of density, plasma potential and turbulent autocorrelation time. Afterwards the properties of the $E \times B$ flow are studied analysing the variation of its velocity and shear through the transition to the confined regime. Also a comparison between the turbulent rate and shearing rate during the transition to the H-Mode is presented. An analysis of the time evolution of the flow acceleration against the intensity of the Reynolds stress force is done. The presence of other forces to consider for a complete modelling of the Zonal Flow in case of induced biased H-Mode is reported. Some theoretical hypothesis in accordance with experimental results are presented. Furthermore an additional analysis decomposing the Reynolds tensor in more stresses is done studying the contribution of the turbulences to viscosity in the anomalous transport and the diffusive momentum transfer.
Chapter 5 Conclusions on all the analysis work are presented with proposals on improvements of the Zonal Flow model for stimulated H-Mode with suggestions for future works.

Contents

Chapter 1

Introduction

For several years we have being looking for new sources of renewable energy. It is a necessity of a continuously growing society at present mostly sustained from fossil fuels. Although this kind of sources could last for many years, sooner or later it will be depleted. A new type of renewable power has to be found.
From the half of last century a pioneering way to supply energy useful to mankind is studied. New researches have been done with the aim to achieve a breakthrough source of energy thanks to thermonuclear fusion.

The purpose of this thesis is to study the reduction of turbulences in plasma physics through the transition to the High confinement Mode. A turbulence is a perturbation of a system out of equilibrium which leads to a state of absence of predictive capability. In this work self organising plasma mechanisms are studied and their relation with this improved regime. It is made possible thanks to deuterium D-shaped discharges in Upper Single Null configuration with edge biasing induced H-Mode in RFX-mod tokamak.

1.1 Physics of Nuclear Fusion

The plasma is a state of matter which consists of particles with opposite charge in form of a single ionised gas. The main difference of a plasma from a neutral gas is the interaction among particles which is due to the nature of long-range electromagnetic forces. This kind of collisions, considered elastic collisions, involves the necessity to confine the particles to make them undergo a fusion reaction with the aim of producing the desired energy. This confinement can be done through electromagnetic fields thanks to coils structures that will be explained in chapter 1.3.

The nuclear fusion is at the base of energy production in a collisional process in which two light nuclei are combined to form a heavier nucleus and other particles releasing kinetic energy. This energy is function of the difference between the binding energy of the final nucleus and starting nuclei. As can be observed in figure 1.1 there exists an increasing of binding energy per nucleon for low mass nuclei with consequent production of energy for a fusion process. In particular

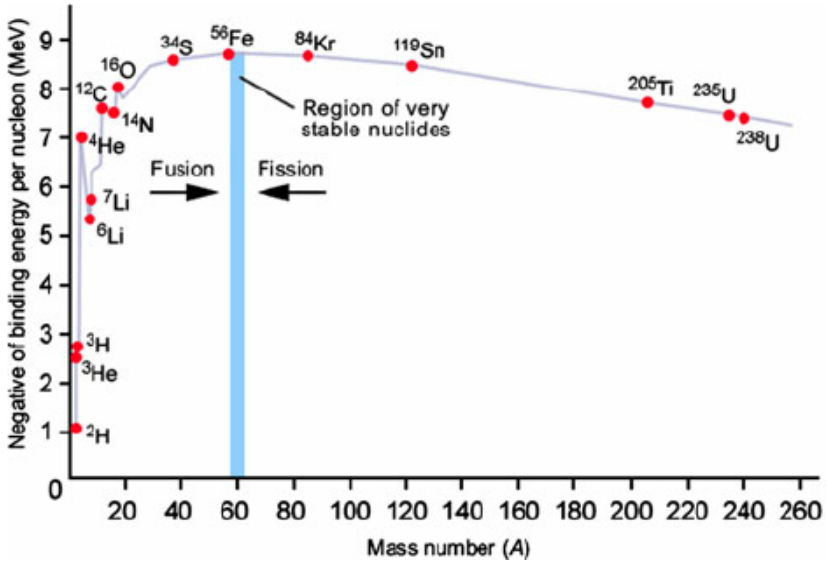

FIGURE 1.1: Binding energy per nucleon as a function of mass number. Taken from [1].

helium nucleus and the isotopes of hydrogen can be considered, among which the most favourable reaction is:

$$^{2}D +^{3} T \longrightarrow^{4} He +^{1} n + 17.6MeV$$

This can be also observed from the cross section of the D-T reaction compared to the other possible ones, as it can be seen from figure 1.2. It is worthwhile to say that in fusion physics either temperature and energy are expressed in eV thanks to the equivalence of 1eV = 11605 K through Boltzmann constant. The considered cross section can be moreover written in another form thanks to an empirical formula as follows:

$$\sigma(E) = \frac{A_5+[(A_4-A_3E)^2+1]^{-1}A_2}{E[exp(A_1E^{-1/2})-1]}$$

where the energy is in KeV and the A_J are named Duane coefficients and they are equal to $A_1 = 45.95, A_2 = 5.02 \cdot 10^4, A_3 = 1.368 \cdot 10^{-2}, A_4 = 1.076, A_5 = 409$ [2, p. 44, 45]. The resulting cross section is in $barns^2 (1barn = 10^{-28} cm^2)$. It can be useful to compute the so called *Reactivity* $< \sigma v >$ where v is the relative velocity of a particle with respect to another one in a two particle interaction system and the $<\cdot>$ symbol expresses an average on spaces and velocities.

As just explained the elements most promising to achieve a thermonuclear reaction are deuterium and tritium. The former can be extracted from sea-water, where it is present in a fraction of 1 part in 6700 hydrogen, and so it is ideally inexhaustible, while the latter decades with a half-time of 12 years hence is necessary to obtain it in an alternative way. The breeding ot tritium is currently done through the transmutation of lithium to tritium thanks to the reactions

$$^{6}Li + n \longrightarrow T +^{4} He + 4.8MeV$$
$$^{7}Li + n \longrightarrow T +^{4} He + n - 2.5MeV$$

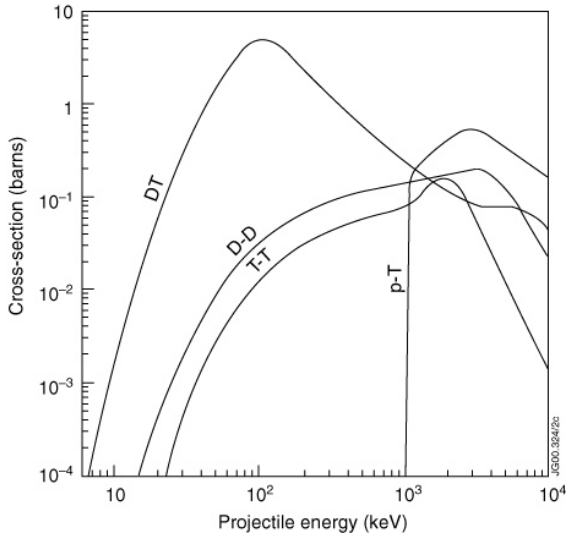

FIGURE 1.2: Fusion reactions cross section. Taken from [3].

They present different cross sections in function of energies of neutrons that interact with Lithium. In a future fusion reactor this process happens in the *blanket*: a multifunctional structure surrounding the vacuum vessel, containing lithium (Li_2O) with the aim of absorbing neutrons to produce tritium with furthermore the roles of shielding the external components of the experimental device and transforming the kinetic energy of neutrons in heat to eventually produce the outgoing electricity thanks to a cooling system.
To obtain a positive production of energy from a thermonuclear process is necessary that the energetic balance is positive considering the energy to initially heat the plasma, the one produced as result of fusion reactions and all the energy lost through different processes of electromagnetic or transport type. Is called *break-even* when the plasma experimental device is in a condition for which the energy produced from thermonuclear reactions is equal to the one required to heat the plasma. Another important condition to consider is the *ignition* in which the power generated from the α particles is sufficient to balance all the losses due to the various processes and the plasma is self-sustained without external heating.
An historical criterion to determine whether a fusion reactor can be considered ignited is the *Lawson criterion*: a condition on the product of density and energy confinement time (which will be explained better discussing the importance of H-mode in chapter 2.1); this latter seems to be higher for deuterium plasma with respect to hydrogen one [4]. At present is used more an inequality based on another product which takes into account also the temperature named *triple product* $nT\tau_E$. The physical values that are intended to be reached are $nT\tau_E \sim 10^{21}(m^{-3}KeVs)$ at $T \sim 10KeV$.

1.2 Magnetohydrodynamics

The plasma can be properly described in the framework of Magnetohydrodynamics (MHD). It was born as development from the fluid dynamics considering also the contribution of the electromagnetic field taking into account the interactions between charged particles.
This section will introduce the basics of fluid and magnetohydrodynamics. Going into details would be beyond the scope of this thesis. The formulation of the theory treated in this section is taken from [5].
Since the eighteenth century physicists and mathematics studied the principles which rule the fluid dynamic leading to a full set of equations:

$$\frac{\partial \rho}{\partial t} + \nabla \cdot (\rho \mathbf{v}) = 0 \tag{1.1}$$

$$\frac{\partial \mathbf{v}}{\partial t} + (\mathbf{v} \cdot \nabla)\mathbf{v} = -\frac{1}{\rho}\nabla p + \mathbf{F} + \frac{\mu}{\rho}\nabla^2 \mathbf{v} \tag{1.2}$$

$$\rho(\frac{\partial \epsilon}{\partial t} + \mathbf{v} \cdot \nabla \epsilon) - \nabla \cdot (K \nabla T) + p \nabla \cdot \mathbf{v} = 0 \tag{1.3}$$

These equations are respectively the *equation of continuity* (1.1), the *Navier-Stokes* equation (1.2) and the *energy* equation (1.3) and they describe the *hydrodynamics*.
Here μ is the *viscosity* which expresses the magnitude of the off-diagonal part of the second-rank tensor P_{ij} of surface forces inside a fluid and hence it actually represents the relative motions amongst layers of a fluid. It can be also considered as $\nu = \mu/\rho$ named *kinematic viscosity*. p is the magnitude of the diagonal part of the same tensor usually known as *pressure*, while K is the *thermal conductivity*. These two terms are taken into account in the equations when is considered the transport phenomena with a distribution slightly different from of a Maxwellian. Finally $\rho = mn$ is the mass density, ϵ the energy, v the fluid velocity and $\mathbf{F}$ an eventual external force.
In the concept of fluid "dynamics" is important to consider the variation of physical quantities along a fluid element and it appears through the *material derivative* named also *convective derivative* or *Lagrangian derivative*:

$$\tfrac{d}{dt} = \tfrac{\partial}{\partial t} + \mathbf{v} \cdot \nabla.$$

The fluid dynamics equations had been obtained either from microscopic considerations either from macroscopic too, that confirmed their validity even though a mathematical solution of them is still an open problem, in particular for Navier-Stokes equation.
A relevant equation for the theory regarding this thesis is the *vorticity equation*:

$$\frac{\partial \omega}{\partial t} = \nabla \times (\mathbf{v} \times \omega) + \nu \nabla^2 \omega, \tag{1.4}$$

where $\omega = \boldsymbol{\nabla} \times \mathbf{v}$ is named *vorticity*. This equation expresses the variation in

time and space of eddies structures and the possibility of their formation or destruction. In particular an increment due to "anomalous" or turbulent transport can be seen in the increasing of the viscosity ν [6]. The second term of R.H.S. of (1.4) can be completely removed in case of an incompressible fluid or a barotropic fluid. In the first case we have $\nabla \cdot \mathbf{v} = 0$ and in the second case the pressure is directly function of density ($p = p(\rho)$). In both cases it takes to the same mathematical result. One term could be neglected with respect to the other one also in case of highly viscous fluid or at the opposite ideal fluid, in particular in function of the *Reynolds number* $R = \frac{LV}{\nu}$, where L is the typical length of a tube that fluid passes or an object immersed into the fluid and and V the fluid velocity.
Needless to say that Magnetohydrodynamics requires Maxwell's equations:

$$\begin{gathered}\nabla \cdot \mathbf{E} = \frac{(n_i - n_e)e}{\epsilon}, \\ \nabla \cdot \mathbf{B} = 0, \\ \nabla \times \mathbf{B} = \mu(n_i \mathbf{v}_i - n_e \mathbf{v}_e)e + \frac{1}{c^2}\frac{\partial \mathbf{E}}{\partial t}, \\ \nabla \times \mathbf{E} = -\frac{\partial \mathbf{B}}{\partial t},\end{gathered}$$

where $(n_i \mathbf{v}_i - n_e \mathbf{v}_e)e$ represents the current density in function of electrons fluid and ions fluid densities and velocities.μ and ϵ are respectively the magnetic permeability and the electric permittivity.
The thought which lies at the basis of MHD is that the plasma is taken in a condition in which the charge separation between electrons and ions can be neglected bringing to the *one-fluid model*. In this model the previous two-fluid variables are combined together to obtain new equations in a form similar to the original one. As example $\mathbf{v} = \frac{m_i \mathbf{v}_i + m_e \mathbf{v}_e}{m_i + m_e}$ and $\rho = n(m_i + m_e)$ are respectively the velocity and the density of the overall fluid.
There exists an equation which relates the one-fluid current density $\mathbf{j} = ne(\mathbf{v}_i - \mathbf{v}_e)$ to the fluid velocity and both electric and magnetic fields:

$$\mathbf{j} = \sigma(\mathbf{E} + \frac{\mathbf{v}}{c} \times \mathbf{B}), \tag{1.5}$$

where σ is the *electrical conductivity*. It is named *Ohm's law*. The (1.5) is actually a simpler form of the equation known as generalized Ohm's law which considers also other contributes multiplied by electron mass which are often neglected. Although this equation is necessary to derive the fundamental equations of one-fluid model, it does not constitute one of the complete set of the magnetohydrodynamics because in the MHD model is often used the non relativistic approximation which permits to consider the electric field as an independent variable and hence to obtain from Maxwell's equations and Ohm's law:

$$\nabla \times \mathbf{B} = \mu \mathbf{j}, \tag{1.6}$$

$$\frac{\partial \mathbf{B}}{\partial t} = \nabla \times (\mathbf{v} \times \mathbf{B}) + \lambda \nabla^2 \mathbf{B}, \tag{1.7}$$

where $\lambda = \frac{1}{\mu\sigma}$ is the *magnetic diffusivity*. The equation (1.7) is named *induction equation* and it relates the time derivative of magnetic field with fluid velocity

and both magnetic field spatial variations and it could be considered the "equivalent" of vorticity equation (1.4) for Magnetohydrodynamics. The extreme cases in which one of the two terms of R.H.S. of (1.7) are neglected can happen also here as for vorticity equation (1.4). Here is function of the magnetic diffusivity λ or alternatively the electrical conductivity σ, to distinguish the cases of weakly or highly conductive plasmas. It can also be defined the *magnetic Reynolds number* $R_M = \frac{LV}{\lambda}$, where L and V have the same meaning of Reynolds number.
Adding the contribute of magnetic field to the Navier-Stokes equation (1.2) also thanks to equation (1.6) is obtained

$$\frac{\partial \mathbf{v}}{\partial t} + (\mathbf{v} \cdot \nabla)\mathbf{v} = -\frac{1}{\rho}\nabla p + \mathbf{F} + \frac{1}{\mu\rho}(\nabla \times \mathbf{B}) \times \mathbf{B} + \nu\nabla^2\mathbf{v}. \tag{1.8}$$

This equation is usually referred to as momentum balance equation. Here μ is the magnetic diffusivity coming from equation (1.6). The contribute of electromagnetic field has to be included also to energy considerations and this brings to an equation identical in form to (1.3) with the addition of an ohmic heating term j^2/σ.
Eventually the continuity equation can be expressed in function of the one-fluid model variables obtaining the same identical form of (1.1).
All this lead to a new complete set of equations: the *continuity* (1.1) and *energy* (1.3) equations expressed with one-fluid variables as just explained, the *induction* equation (1.7) and equation (1.8).
This describes the physics of electromagnetic fluids named *Magnetohydrodynamics*. A fluid which satisfy this full dynamical theory is named *magnetofluid*.

1.3 Tokamak

Thanks to its complex structure the RFX experiment allows to be exploited also as Tokamak. A tokamak is a fusion reactor configuration based on a toroidal structure with a system of coils to regulate the electromagnetic fields for maintaining concentrated the plasmas. In the tokamak there exist a lot of structures to heat the plasmas in a controlled way and to achieve the energy produced from the reactor at present in form of heat. All this is complemented by safety structures to avoid the warm plasma to damage the building (figure 1.3).
The acronym tokamak is the Russian transliteration of "*to*roidal'naya *ka*mera s *ma*gnitnaya *ka*tushka" which stands for "toroidal chamber and magnetic coils".

1.3.1 Plasma Heating methods

To reach the ideal temperature condition inside the reactor the plasmas needs to be heated. It can be initially done through the plasma current which generates

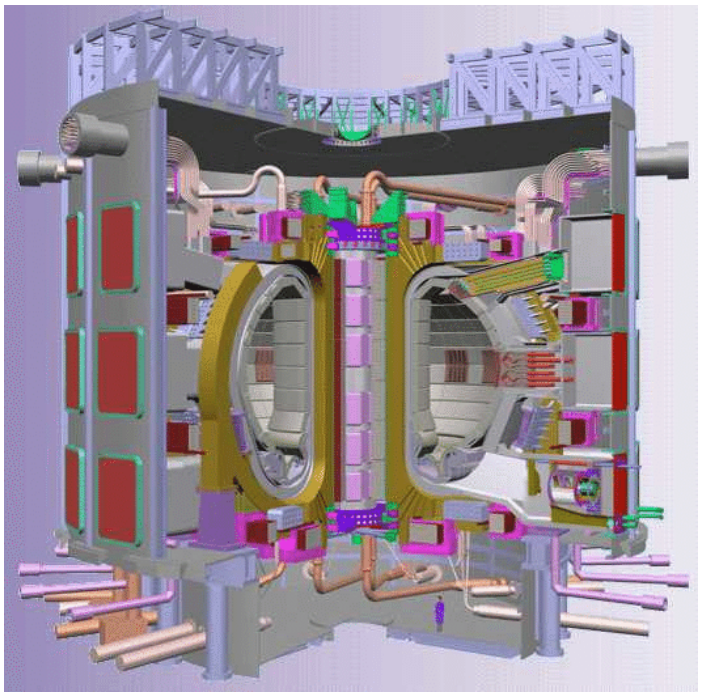

FIGURE 1.3: Tokamak structure of ITER project. Taken from [7].

the poloidal field, process named *ohmic heating*. This process results to be not sufficient to warm enough the plasma to the desired temperature. It is due to the inverse dependence of plasma resistivity with respect to the temperature. Therefore the attainable temperature with this method is below 10 keV. Even though some proposals of high field machines had been done to reach this scope, at present it seems not possible heating the plasma with the only ohmic heating.
It is clear the necessity of additional heating methods. The possible ones are provided from injection of neutral atoms or use of radio frequency waves.
The first method is based on acceleration of charged ions which are subsequently neutralised through exchange reactions in a specific chamber thanks to a neutral gas. Hence energetic ions are obtained to then inject them into the plasma. Eventually they are ionised through interactions with plasma particles yielding energy to the plasma itself. This process is named *Neutral Beam Injection (NBI)*. The beam direction is preferably tangential to the fusion device, but it has to be a compromise also in function of the available space between toroidal field coils. The tangential direction is useful to pass neutral ions momentum to the plasmas.
The second type of additional heating is provided by electromagnetic radiations by harnessing resonance conditions resulting in absorbed energy from the plasmas. It happens thanks to a high power generator distant from plasmas, a low losses transmission and a radio frequency coupling system. The main methods based on this procedure are the *ion cyclotron resonance heating (ICRH)* and *electron cyclotron resonance heating (ECRH)*. They exploit wave frequencies close to cyclotron frequency of ions or electrons which are respectively in the range of 30-120 MHz and 100-200 GHz.

1.3.2 Electromagnetic configuration

The coordinates system of a tokamak is illustrated in figure 1.4. R defines the radial direction of the torus in cylindrical coordinates while φ is the toroidal direction and z the height. The second coordinate system, located in R_0, is given by: r as radial direction with a maximum radius, θ and eventually another coordinate z as height of cylindrical coordinates along the φ coordinate of the torus.
The basic reasoning of plasma confinement in a reactor is the exploitation of strong magnetic fields to keep particles moving along close circular orbits lying on a plane perpendicular to the field lines. The radial limited region which defines the confinement is the *Larmor radius*:

$$r_L = \frac{mv_\perp}{qB},$$

where r_L and $v_\perp$ are along the minor radius direction. Therefore particles rotate around their *guiding centre* which at the same time translates with constant velocity in the *toroidal direction* around the centre of the tokamak.
The first reactors were born with cylindrical linear shape as a giant system of coils where particles at the end of the linear reactor were partially confined employing the *mirror* effect. It is a phenomenon for which in presence of a region of increasing magnetic field particles are reflected back. The linear reactors were abandoned years later because of instabilities and problems of different nature.
To avoid particle losses at the end of linear devices a close toroidal shape has been conceived indeed the tokamak. Despite of this solution the toroidal structure involves some problems originated from radially decreasing intensity of the confinement magnetic field: the *gradient drift* and *curvature drift* effects. The former happens because of the non uniform of the magnetic field; the latter is a consequence of centrifugal forces which particles undergo rotating around the centre of the tokamak. These two effects cause a vertical displacement of particles in the poloidal direction because both field gradient and centrifugal forces are radially directed:

$$\mathbf{u}_{g.c.} = \frac{c}{q}\frac{\mathbf{F}\times\mathbf{B}}{B^2} \tag{1.9}$$

where $\mathbf{F}$ is the force due to the gradient of magnetic field or the centrifugal force and $\mathbf{u}_{g.c}$ the velocity of a single guiding centre. Therefore the guiding centres are vertically shifted. However the particles move in opposite direction depending on whether they are positively or negatively charged. Hence it produces a poloidal electric field.
This field together with the previous toroidal magnetic field, produces another displacement, always following equation (1.9). This inherent behaviour needs a correction to avoid now that particles radially drift hence another poloidal magnetic field is created to prevent particles to ruin the reactor chamber and remain confined. The combination with the previous fields with this new one moves the guiding centre upon and above the median horizontal plane with a helicoidal

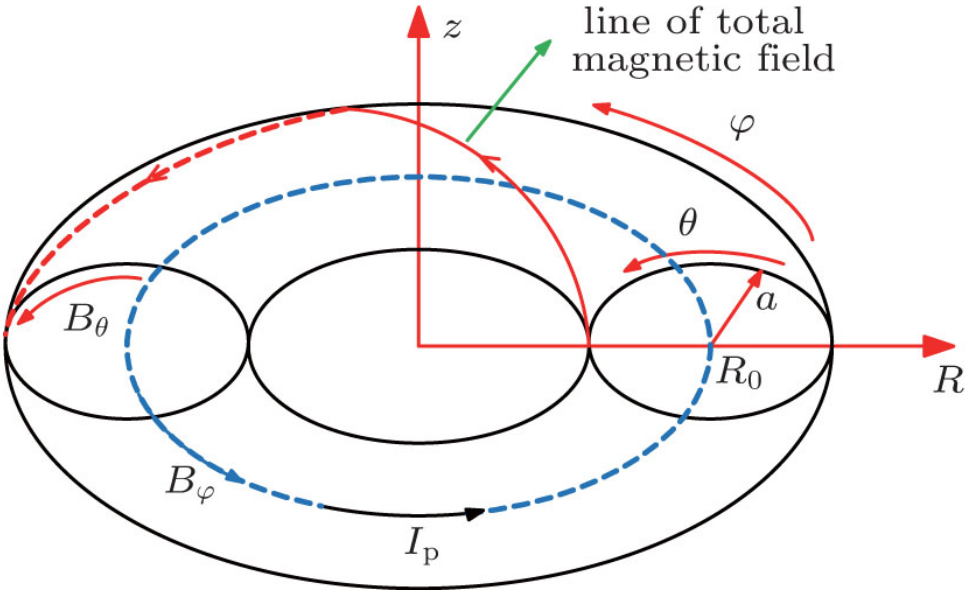

FIGURE 1.4: Coordinates system of a Tokamak. B_ϕ is main toroidal field, B_θ is poloidal field. I_p is the plasma current. Taken from [8].

motion too. With this procedure is said that the field is provided with a *rotational transform*.

Although all these procedures is really hard to perfectly confine the plasma around the centre of cylindrical section of the torus hence, to avoid that too many particles exceed the confinement, in the external region of the plasma there are some structures done to handle the impurities originated due to many physical reasons as adsorbed material from the surfaces or sputtering. These losses have to be taken into account also for the continuous recycling of particles that constitute or heat the plasma. These structures are specific surfaces named *target*: they intercept the field lines to avoid that the energetic particles go to borders of the chamber; they are divided into limiters and *divertors*. The former are solid objects that come out of the surfaces to create a local area to prevent that particles to reach the borders, the latter are a set of plates with specific coils system to ensure that there is a spot of null poloidal field named *X-point* (figure 1.5). The RFX works in a X-point configuration also named *single-null*.

The presence of a local magnetic field which deviates particles from the borders lead to creation of a safe layer named *Scrape Off Layer* (SOL). The radially largest magnetic surface which is directed to the X-point is the *Last Closed Flux Surface (LCFS)* or *separatrix*. It defines the region of the SOL and all the particles external to the LCFS goes towards the divertors and will not perform a full toroidal orbit. The X-point or null is important to the purpose of this thesis because it had been proved in lot of experiments that the single-null configuration with only one X-point and the gradient of the magnetic field directed towards the X-point is more favourable for the transition to High confinement mode [9]. The data used for the thesis had been taken in this configuration.

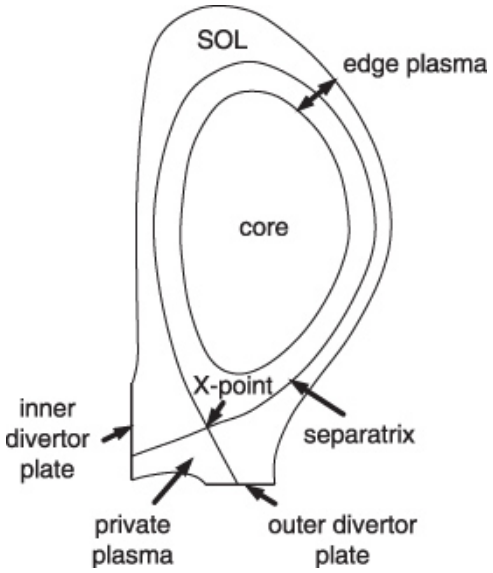

FIGURE 1.5: Divertors system in poloidal section. In the image is represented a single null configuration. Taken from [10].

There exists an equality which the defines the toroidally uniform surfaces of magnetic field in a plasma device permitting to establish some flux functions that express the contour lines of the magnetic field. This equation is the *Grad-Shafranov* equation. The physical measurement necessary to define the mathematical boundary conditions of Grad-Shafranov equations are done through a third system of coils parallel to plasma current to determine its position and shape.
Another important factor for plasma devices is the *safety factor q* which describes how much the magnetic lines are enveloped around the torus:

$$q = \left\langle \frac{d\phi}{d\theta} \right\rangle \simeq \frac{rB_\varphi}{RB_\theta}.$$

The second approximation holds for tokamak devices. It can be seen as the toroidal angle that a field line travels performing an entire poloidal orbit. The value of safety factor at different radius plays an important role in the plasma instabilities.
Last but not least the *Beta* factor:

$$\beta = \frac{p}{B^2/2\mu_0}$$

which is the rate between the kinetic energy of the plasma and the magnetic pressure of field that confines it, hence it defines the efficiency of the confinement of the plasmas.

1.3.3 Alternative experimental devices

The other main configurations used as plasma physics experiment are *Reversed Field Pinch* and *Stellarator*.
The RFX-mod experiment is a plasma reactor born as Reversed Field Pinch(RFP) configuration reactor hence the name "Reversed Field eXperiment".

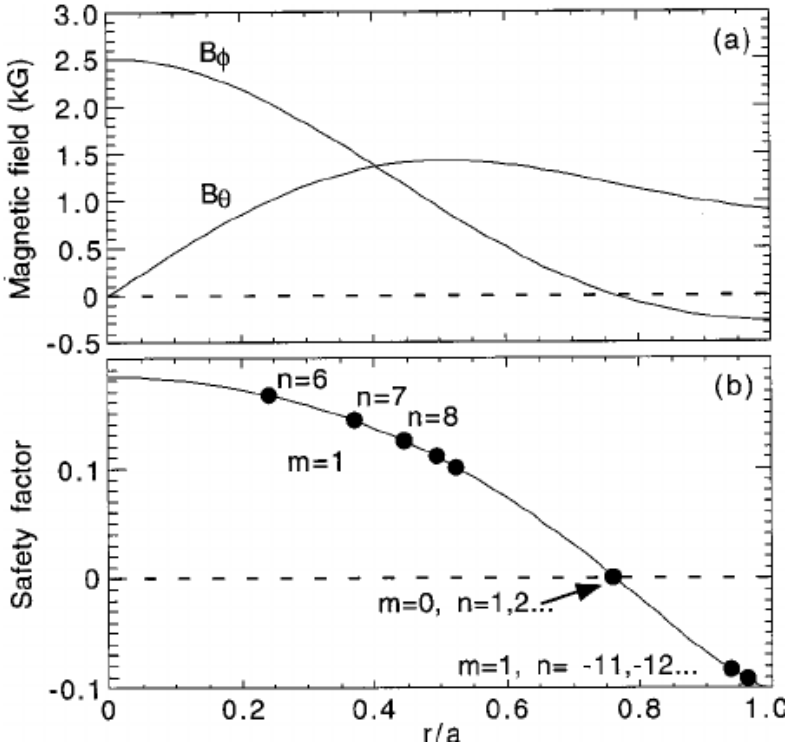

FIGURE 1.6: Reversed Field Pinch magnetic field components and safety factor. Taken from [11].

The RFP has the same toroidal structure of the tokamak but presents a particular behaviour as regards the toroidal magnetic field for the outer region of the plasma where the field changes its sign from which the name "reversed". In this region the poloidal field dominates. The inversion of toroidal field implies a strongly paramagnetic behaviour of the plasmas inside the device because the field trend is decreasing with the increasing of the minor radius r. It implies also negative values of safety factor q (figure 1.6).
The stellarator is a plasma device which permits to obtain a rotational transform without the necessity of using more magnetic fields thanks to special helicoidal coils outside the plasma in the *torsatron* scheme or a structure of deformed coils. The absence of the plasma current lead to real stable operating conditions but obviously their construction is considerably complicated as it can be seen in figure 1.7.

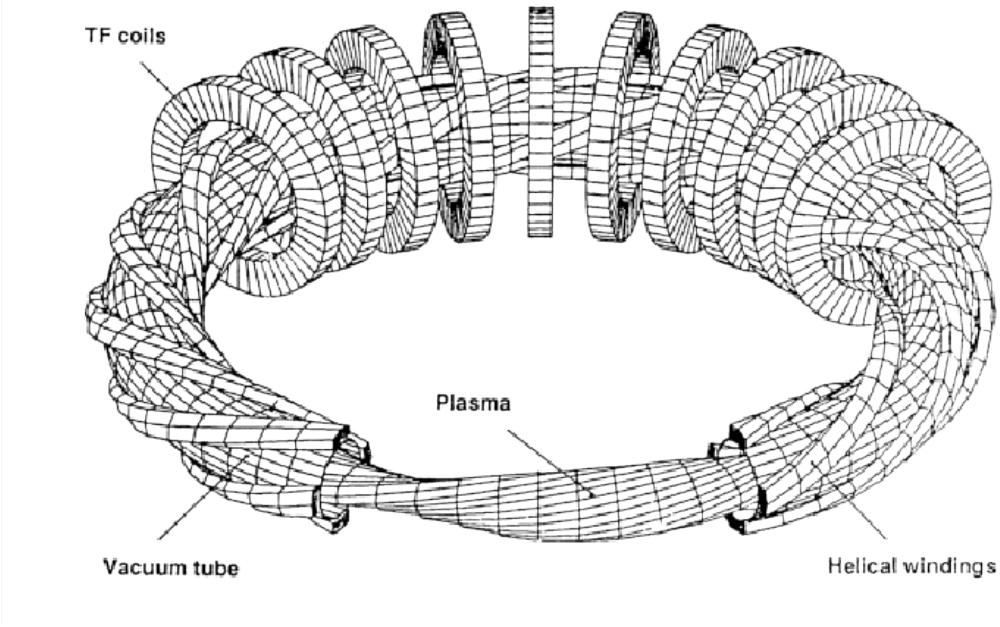

FIGURE 1.7: Stellarator coils configuration. Taken from [12].

Chapter 2

High Confinement Mode

Was on 4 February 1982 when the German physicists Fritz Wagner was faced with an unexpected changing in the physical properties on the edge of plasma experiment he was working on. A regime with improved confinement properties has been observed during experiments with applied momentum torque through Neutral Beam Injection, with improved confinement properties. It happened in the ASDEX experiment at the Max Planck Institute for Plasma Physics (IPP, in Garching, Germany) [13].
This was afterwards named *High Confinement Mode (H-Mode)*.
The H-Mode is characterised by many physical aspects as steeper pressure gradients, increasing of particles and energy confinement time, with increasing temperature and radial electric field and many others. All these aspects can assure that the plasma is in this better confined condition, nevertheless the main phenomenon which defines the physics at the basis of the H-Mode is not still clear. One evident consequence of the transition to the H-Mode is the turbulences reduction. One hypothesis of this behaviour is ascribed to the action of *Reynolds stress*.

2.1 H-Mode

This section will describe the main properties of the H-mode, highlighting the differences with respect to the previous regime that was thereafter named Low confinement Mode(L-Mode).
The main importance of the H-Mode is the improvement of the confinement time τ_E, introduced in chapter 1.1.
An useful quantity that can be considered is the ratio between the confinement time in H-Mode and the one in L-Mode named *H factor*:

$$H = \frac{\tau_E^{H-Mode}}{\tau_E^{L-Mode}}$$

which can reach values up to 4 [14].
Initially the H-mode was achieved through the injection of tangential neutral beam power, which increased the total amount of power delivered to the plasma as well as provided an additional source of momentum. Reproducing this led to the possibility of creating scaling laws for the power threshold mainly depending

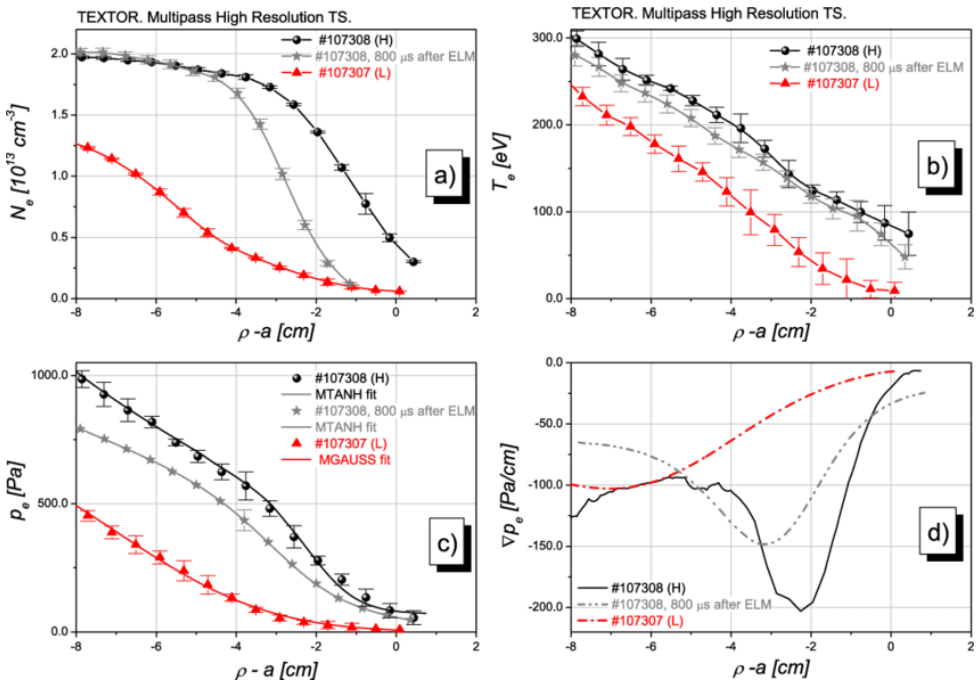

FIGURE 2.1: Physical quantities before ad after transition to H-Mode in TEXTOR: a) electron density b)temperature c) pressure and d) pressure gradient. Taken from [17].

on the intensity of the toroidal field and the density, secondly a weak dependence on the sizes of the plasma device [15].
The features which defines the physics of the H-mode at the edge of the plasmas are the following:

- increasing of radial *electric field** and consequent *flow velocity*
- increasing of velocity *shear*
- formation of an external *transport barrier*, with a strong *pressure pedestal* thanks to the increase of temperature and/or *density gradient*
- in some cases formation of *Internal Transport Barriers* (ITBs) with related turbulences reduction also in core region

Some of them are illustrated in figure 2.1. Since the physics which regulates the generation of H-Mode is not totally defined this process could be described from other points of view. Nevertheless these physical aspects are commonly observed in different devices [18–21].

*The electric filed which characterises a magnetised plasmas is of ambipolar nature. An ambipolar electric field is a field generated due to imbalances between electron and ions densities due to a pressure gradient or an external electric field. It is a steady state in which the system is rebalanced from charged particles diffusion with equal number density fluxes known as *ambipolar diffusion* against a background of neutral atoms.
In a simple way it can be expressed as

$$E = \frac{D_i - D_e}{\mu_i + \mu_e} \frac{\nabla n}{n},$$

where $D_{i,e}$ and $\mu_{i,e}$ are respectively *diffusion coefficient* and the *mobility* of ions and electrons [5].

The increasing of the shear suggests a variation in the $E \times B$ velocity and hence a contribution in the acceleration along the $E \times B$ direction as can be seen looking at the momentum balance equation (1.8). It had been discovered that the H-Mode can also be induced with an external electric field instead of exceeding the heating power [18, 21]. This is the case of the RFX-mod experiment hence the data used for the analysis of this thesis. Furthermore steeper ion saturation current profiles have been reported for the H-Mode with respect to the L-Mode [4, 21]. Being this signal related to the electron density current it highlights the formation of transport barriers. An additional feature is the plasma impedance increase during the H-Mode [21] probably related to the strong modifications of temperature and density.
There are also some other interesting aspects that are beyond the scope of this thesis but are worth to be mentioned because of their possible purpose in the search of a complete understanding of the confined regime. One of them is the evidence of modulation of the plasma inductance due to edge barrier formation and steepening of pressure gradient in the so called Limit Cycle Oscillations (LCO) [19]. Another issue, more interesting from the standpoint of this thesis, regards the biased induced H-Mode in RFX-mod experiment where an hysteresis-like behaviour between the L-Mode and what is named 'post H-Mode', when the electrode is switched off, has been reported [21]. It can suggest a possible subject of investigation based on which physical quantities endure this hysteresis maintaining the enhancements gained during the H-Mode.

2.2 Zonal Flow and Reynolds Stress

2.2.1 Zonal Flow theory and turbulences reduction

When the plasmas is perturbed by a pressure or density gradient a response is generated in the perpendicular direction due to a diamagnetic current to establish the equilibrium. This happens both for ions and electrons and lead to what are known as ions and electrons *diamagnetic drift waves*.
In the direction perpendicular to the magnetic field the drift turbulence propagation is characterised by a spatial scale $\rho_S \equiv C_S/\Omega_{C_i}$, as rate of ion sound speed and ion gyro-frequency, and a drift wave number such that $k_{//} \ll k_\perp$. A non linear transfer of energy occurs depending on the range of the product $k_\perp \rho_S$ characterising different kind of drifts, according also to temperature and density of the plasmas [18].
In the 1979 Hasegawa *et al* found that the drift turbulence kinetic energy with perpendicular wave number $k_r \rho_S \sim 0.1 - 0.3$ condensed into an ordered anisotropic flow with a scale length comparable to the turbulences one in the same direction while in the direction transverse to this latter the scale length was long i.e. $k_\theta \rho_S \sim 0$ in the poloidal direction. Considering the electric field due to the drift wave, these streamlines of $E \times B$ drift can represent regions in which the turbulences are reduced. These closed $E \times B$ iso-potential contours was named *Zonal Flows*.

These contour structures seem to not develop in density fluctuations.
Waves like the ones which propagates through Zonal Flows is known being characterised by ion heat transport due to large ITG (ion temperature gradient) that if increases can lead to ITG drift wave instability [18]. Hence the increasing of temperature gradient and electric field too during the H-Mode led to an enhanced $E \times B$ flow which reduces the turbulences.
The ZFs velocity behaviour can be expressed through the equation

$$\frac{\partial}{\partial t} V_{ZF} = -\frac{\partial}{\partial r} < \widetilde{v_r}\widetilde{v_\theta} > -\nu_d V_{ZF}, \tag{2.1}$$

where $V_{ZF} =< v_\theta >$ is along poloidal direction and $< \widetilde{v_r}\widetilde{v_\theta} >$ is the Reynolds stress. ν_d represents a collisionality dependent flow-damping rate as a relaxation towards the neoclassical poloidal flow [18, 19].
These ZFs have the property of being toroidally and poloidal uniform with wave number along these directions 0. This uniformity can be proved through a measure of $E \times B$ cross-correlation at different toroidal positions with a zero time lag peak [19, 22].
The occurrence of the H-Mode can be seen also from the increment of radial derivative of the $E \times B$ velocity named *shear decorrelation rate* $\omega_{E\times B}$. If this quantity definitively exceed the *natural turbulent decorrelation rate* ω_D the transition to the H-Mode is initiated:

$$\tfrac{\partial}{\partial r} v_\theta \equiv \omega_{E\times B} > \omega_D \equiv \tfrac{1}{\tau_{AC}},$$

where τ_{AC} is the autocorrelation time of turbulences [9, 18, 19, 22, 23].

2.2.2 Reynolds stress as result of perturbed equations

From a mathematical point of view the definition of turbulence comes from the decomposition of the fluid velocity considered in a point into a mean value $\overline{\mathbf{v}}$ and a fluctuation around it $\mathbf{v}'$. The second one can be considered the turbulent velocity field. If then the average is considered it naturally results that $\overline{\overline{\mathbf{v}}} = \overline{\mathbf{v}}$ and $\overline{\mathbf{v}'} = 0$, hence the only terms that stem from these kind of sights on the nature of turbulent fluid are the averages of product components as $\overline{v_i' v_j'}$.
This reasoning can be done to any physical quantity. Hence if we apply it to the entire momentum balance equation (1.8), written in explicit components, it results that

$$\frac{\partial \overline{v_i}}{\partial t} = -\frac{1}{\rho}\frac{\partial \overline{p}}{\partial x_i} + \nu \frac{\partial}{\partial x_j}\frac{\partial}{\partial x_j}\overline{v_i} - \frac{\partial}{\partial x_j}\overline{v_i v_j} - \frac{\partial}{\partial x_j}(\overline{v_i' v_j'}) + \frac{1}{\mu\rho}\left(\epsilon_{jlm}\epsilon_{ijk}\frac{\partial}{\partial x_l}\left(\overline{B_m B_k} + \overline{B_m' B_k'}\right)\right). \tag{2.2}$$

Therefore the additional term that comes out from turbulences contribution is

$$-\tfrac{\partial}{\partial x_j}\left(\overline{v_i' v_j'} - \tfrac{1}{\mu\rho}\overline{B_i' B_j'}\right).$$

It is expressed in S.I. units and in our case the i index represents the radial direction and $\left(\overline{v_i' v_j'} - \frac{1}{\mu\rho}\overline{B_i' B_j'}\right)$ is named *generalised Reynolds stress*.

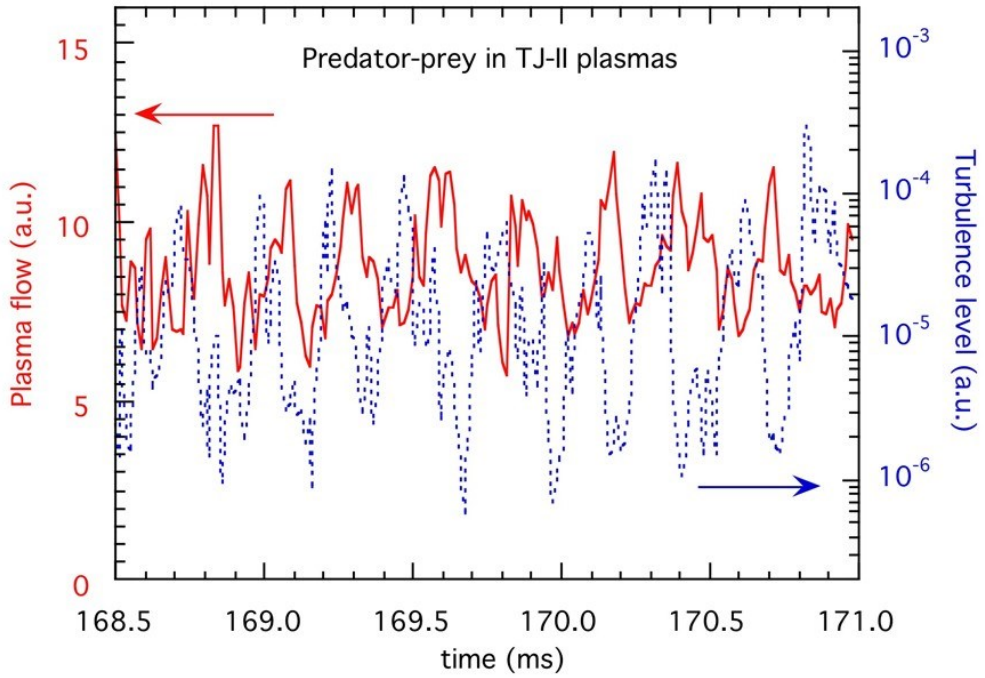

FIGURE 2.2: Predator-prey relationship between Zonal Flows and turbulences in TJ-II stellarator. Taken from [25].

The term $\left(\overline{B_i' B_j'}\right)$ is the Maxwell stress and it has been proved to be negligible compared to the tensor $\left(\overline{v_i' v_j'}\right)$ hereinafter named *Reynolds Stress*.
The dominance of this term occurs in particular for low β cases [6] as for the data used in this thesis.
The quantity $\overline{v_i' v_j'}$ is also expressed with the equivalent notation as $< \widetilde{v}_i \widetilde{v}_j >$.
Furthermore turbulences can appear as eddies structure in the plasma, similarly to what proposed in 1940 from Kolmogorov for fluid dynamics. This aspect has been directly verified in some experiments [19]. One of the effects of the transition to the H-Mode is that this turbulent eddies are elongated along the poloidal direction and broken [6, 18, 19, 21, 23, 24].

2.2.3 Limit Cycle Oscillations

In recent years it has been observed that just before the transition to the H-Mode the intensity of the shear rate against the intensity of the turbulent rate follows a predator-prey model behaviour [9, 22] (figure 2.2).
A predator-prey model is a model in which the two participants evolve in a $\pi/2$ shift phase and it seems to occur to Zonal Flows and turbulences intensities in the phase named *I phase*. These trend between the shearing rate and the turbulent rate is named *Limit Cycle Oscillations*.
The predator-prey behaviour is modelled by Lotka-Volterra equations, applied

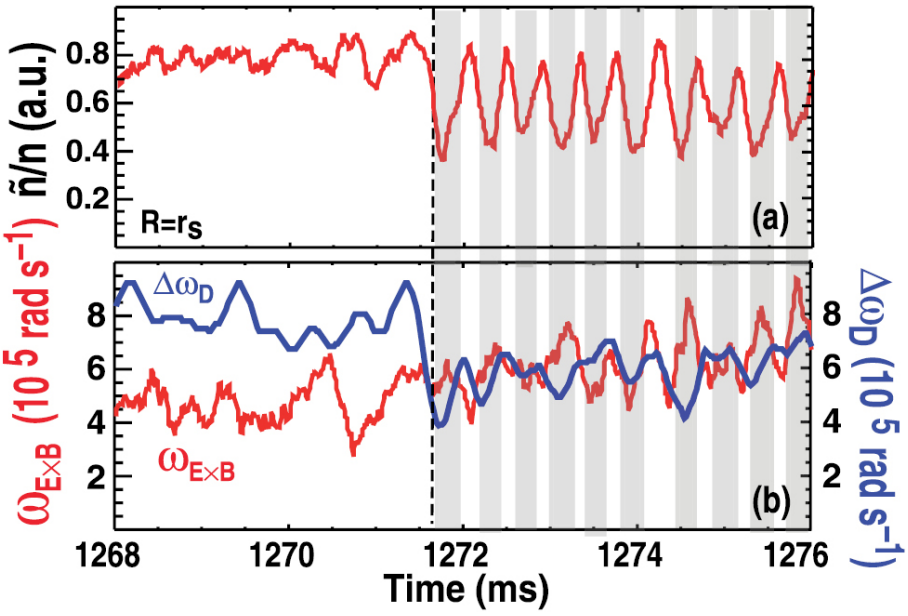

FIGURE 2.3: a) Normalised turbulence intensity b) Shear rate and turbulent rate evolution for L-H transition in DIII-D tokamak. Taken from [19].

in different areas of application as biology, ecosystems, physics, economy and so on. This model consider the presence of a "predator" and a "prey", that in this scenario are respectively the ZFs and the turbulences, that continue to grow and decrease in this $\pi/2$ phase shift against each other.
This sight on the ZF-turbulences interaction lead to another possible way to analyse the turbulence problem. It indeed has been proposed some set of equations to model these LCOs and hence inferring more physical conclusions about the argument [9, 19, 22]. It has been related the turbulence and Zonal Flow kinetic energies with their dissipation rates in a K-ϵ framework. The full description of this model can be found in many articles (e.g. [19, 22]).
The phase shift which characterises the LCOs is featured by an alternation between pressure gradient and turbulence intensity($\tilde{n}/n$) magnitudes with a continuous increasing and decreasing of these conflicting quantities until the ion diamagnetic flow is able to sufficiently grow before the shear flow decays away, at its dissipation rate, and eventually a state of steepened gradient is maintained. It can be seen in particular that at each maximum of shearing rate $\omega_{E\times B}$ corresponds a minimum in fluctuations (figure 2.3).
It has been noticed that the phase shift between turbulences and ZFs maxima increases till it reaches about 180° at the LCO-H-mode transition [19].

Chapter 3

Experimental setup

The data used for this thesis has been collected in the RFX-mod tokamak with deuterium D-shaped discharges in Single Null configurations with edge biasing induced H-Mode.
The RFX-mod has a major radius of R=2m and a minor radius of a=0.459m. The plasma device is provided of a shape feedback control system with an algorithm to obtain the real time ($\sim 1ms$) evaluation of the position of the Last Closed Flux Surface [21] which accuracy had been verified thanks to numerical simulations done with the MAXFEA Grad-Shafranov solver [26].

3.1 Measurement probe

The measurement system used to obtain the data is an advanced Langmuir probe set composed of two boron nitride towers with 40 graphite tips each in an ordered array of 5 tips per column poloidally aligned. The tips have a diameter of 3mm and are 6mm spaced. The distance between the centres of the two towers is 88mm [24]. In addition the probe is equipped with a system of magnetic coils placed inside each tower allowing the simultaneous measurement of the components of magnetic and electric field.
Due to its shape it is called *U-probe*. It is placed at the ϕ= 247°30′ toroidal position, corresponding to 15° toroidally distant from the electrode, kept radially fixed in the radial-poloidal ($r - \theta$) plane.
The position of the U-probe with respect to the minor radius and the average position of the LCFS can be seen in figure 3.2. The tips used to obtain the data for the analysis are the ones represented in figure 3.3. It covers a measurement area of 24mm x12mm per tower with a total space of 24mm x100mm considering also the distance between the two towers.
The physical quantities measured thanks to the U-probe are the following: the floating potentials V_f on the 10 tips of first and last rows of each tower and other additional 2 in the middles for a total of 22 probes, the 6 ion saturation current density signals J_s along some columns and eventually the electronic temperature *Te* inferred with the five pin triple-probe method thanks to the use of 2 electrodes

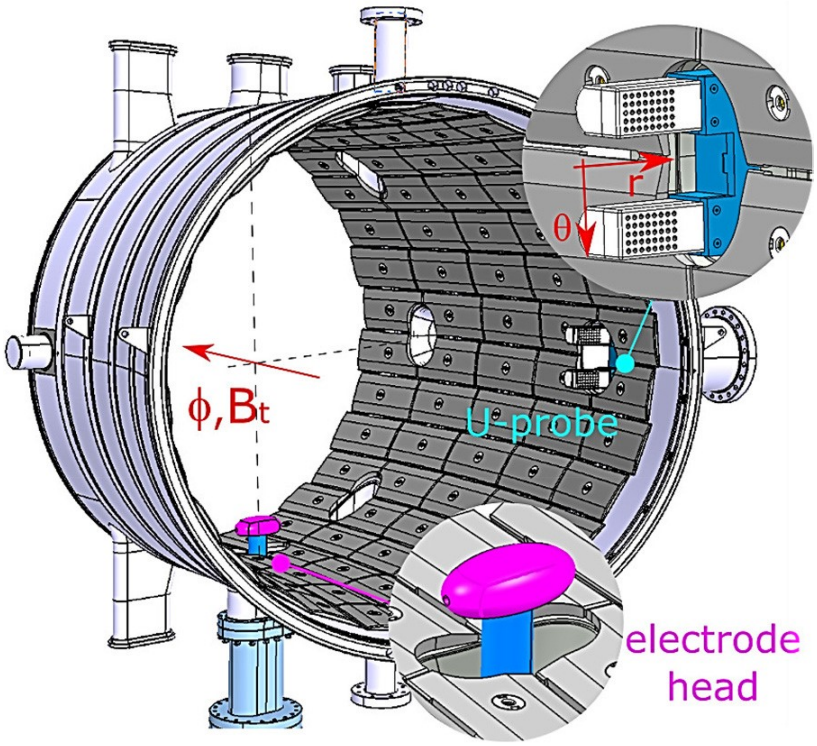

FIGURE 3.1: Edge biasing electrode and measurement U-probe. Taken from [21].

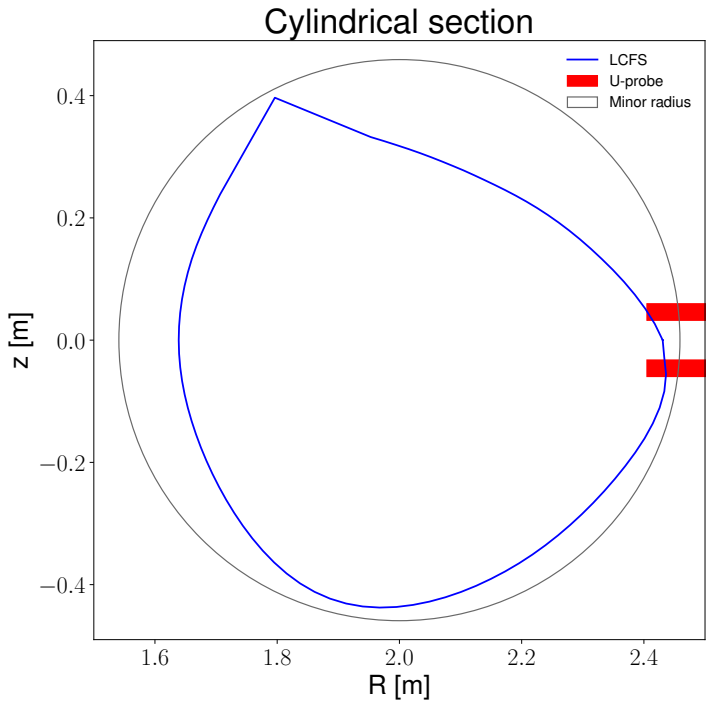

FIGURE 3.2: Cylindrical section of measurement system. The U-probe, the minor radius and a reconstruction of the LCFS are represented.

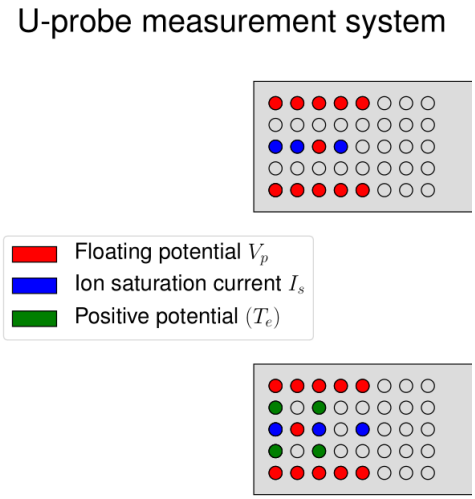

FIGURE 3.3: U-probe measurement system. All tips assigned to a measure are reported: 22 floating potential, 6 ion saturation current columns and 4 fixed positive potential for five pin triple-probe method for electron temperature measurement.

with fixed potentials and other 3 pins to estimate the temperature in 6 radially different positions. How these signals are produced exploiting the Langmuir probe and what they represent is explained in the following section.

3.1.1 Langmuir probe characteristics

A Langmuir probe consists of an electrode inserted in the plasma by means of a support built of insulant material. Its insertion in the plasma influences the plasma itself and it is taken into account in the quantitative measurements through this instrument. If the pin is biased with a varying voltage, from the characteristics I-V curve different plasma quantities can be inferred.
Considering the Debye sheath formed around the probe the current signal presents the trend reported in figure 3.4, in the form

$$I = I_i^{sat}\left[\exp\left(\frac{e(V-V_f)}{K_B T_e}\right) - 1\right].$$

V_f is the floating potential measured from the probe. A floating potential is the potential of a conductor where no net current is collected. Hence this characteristics has to be achieved through a variable potential measurement where V, which is the probe bias, has to be taken from negative values until the plasma potential. For very negative values represents a condition which prevent all the electrons to reach the probe and hence the current measured results to be only due to ions: this is the ion saturation current I_i^{sat}. Furthermore is preferable to not explore in the potential region of electron saturation current for instrument safety reasons.

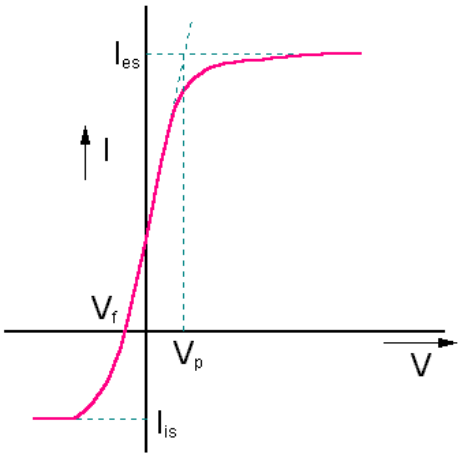

FIGURE 3.4: Langmuir probe I-V characteristics. Taken from [27].

The ion saturation current is related to the plasma density through the expression:

$$I_i^{sat} = 0.5eAnc_s, \tag{3.1}$$

where A is the area of the probe, n is the density and $c_s \simeq \sqrt{\frac{ZT_e}{m_i}}$ the ion sound velocity. Hence from the measure of this quantity is possible to achieve the density once the electron temperature is known.
The temperature measurement is based on the five-pin balanced triple probe method [28]. The triple-probe method is based on the use of two contiguous electrodes biased in relation to each other, technique named double-probe, and a third electrode such that the double-probe is at fixed voltage much greater than the expected values of electron temperature, where the third electrode measures a floating potential. The five pin triple-probe method is an enhancement of the triple-probe method based on the average on two floating potential to reduce the error contribution from the poloidal distribution of the probes.

3.2 Biased stimulated H-mode

As introduced in 2.1, the H-Mode has been induced due to a generated electric field. It has been done thanks to a biasing electrode inserted in the edge of the plasma.
The electrode head is made of graphite and has an ellipsoid shape of the dimensions of 115mm x25mm x65mm and it is positioned 8 cm inside the LCFS (figure 3.1) corresponding to $R/a \approx 0.83$. It is inserted from the bottom of the chamber at the toroidal position of ϕ= 262°30′.
For the analysed discharges the intensity of the voltage produced from the electrode was -300 V. The I-V characteristics of the system has been studied and has been observed to follow a Langmuir probe characteristic with a tendency to saturation with a mainly ion current [21]. This is reported in figure 3.5. This working condition seems to allow more reproducibility of the confined regime.

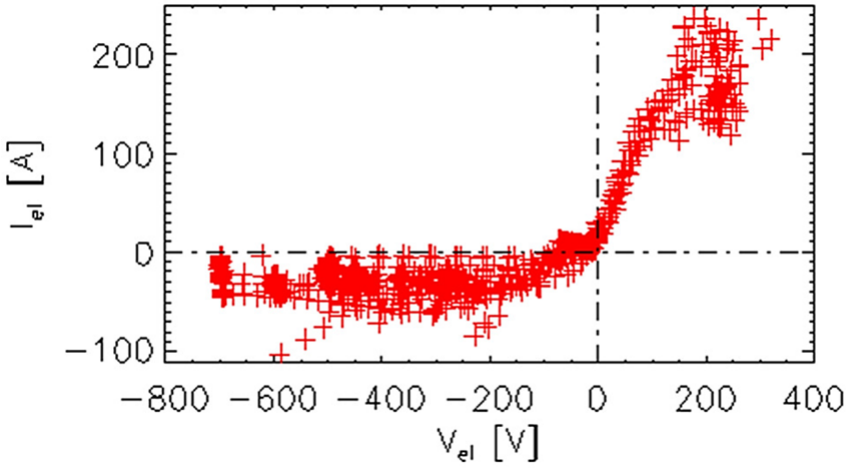

FIGURE 3.5: Characteristics I-V of biasing electrode. Taken from [21].

3.3 Analysed discharges

In the analysed discharges the plasma current is $\leq 50kA$ with a central line averaged density within the range $(2-6)\cdot 10^{18}\, m^3$. The magnetic field on axis is of 0.55 T [24].
The safety factor is in the range of $q_{95} = 3 - 4.5$ as reported in figure 3.6. A multi-chord passive Doppler spectroscopy diagnostic allowed to know in similar experiments that the impurity flow, in particular for C III impurities, that it is localised in the last 5 cm of the plasma edge with the same direction of electron diamagnetic drift.
The full plasma discharge lasts about 1 s. The determination of the L-H transition time interval has been done considering the shape of the D_α signal which is proportional to particle recycling and this is related to plasma flux incident at the edge hence a reduction of this signal suggests a reduction in transport. It can be noticed, as in figure 3.7 with an example of a considered shot, that the ignition of the electrode causes suddenly the reduction of the D_α signal hence it is a simple but reasonable marker of the beginning of the H-Mode that will be subsequently verified with the complete analysis. The central density increases too, but with a little delay sustaining the theory that the transition to the H-Mode is related to a phenomena which start at the edge of the plasma and retro-propagates inside after [18]. Also the soft x-ray (SXR) radiation vertical signal is reported. Its width increment through the H-Mode transition indicates a density increase too [21]. In function of the aim of the thesis it has been considered a time window from just before the transition to immediately after the transition, with a precision of $10^{-2}s$.

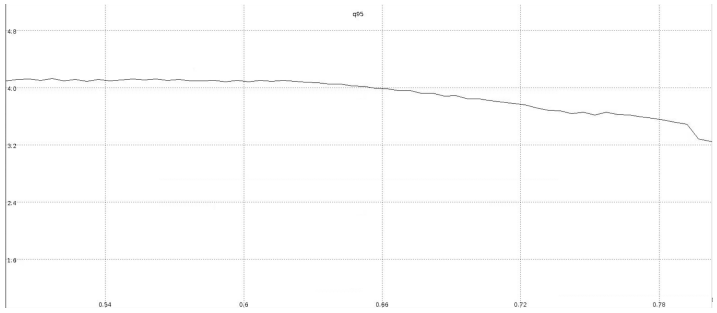

FIGURE 3.6: Safety factor at $R/a = 0.95$. Acquired directly from data.

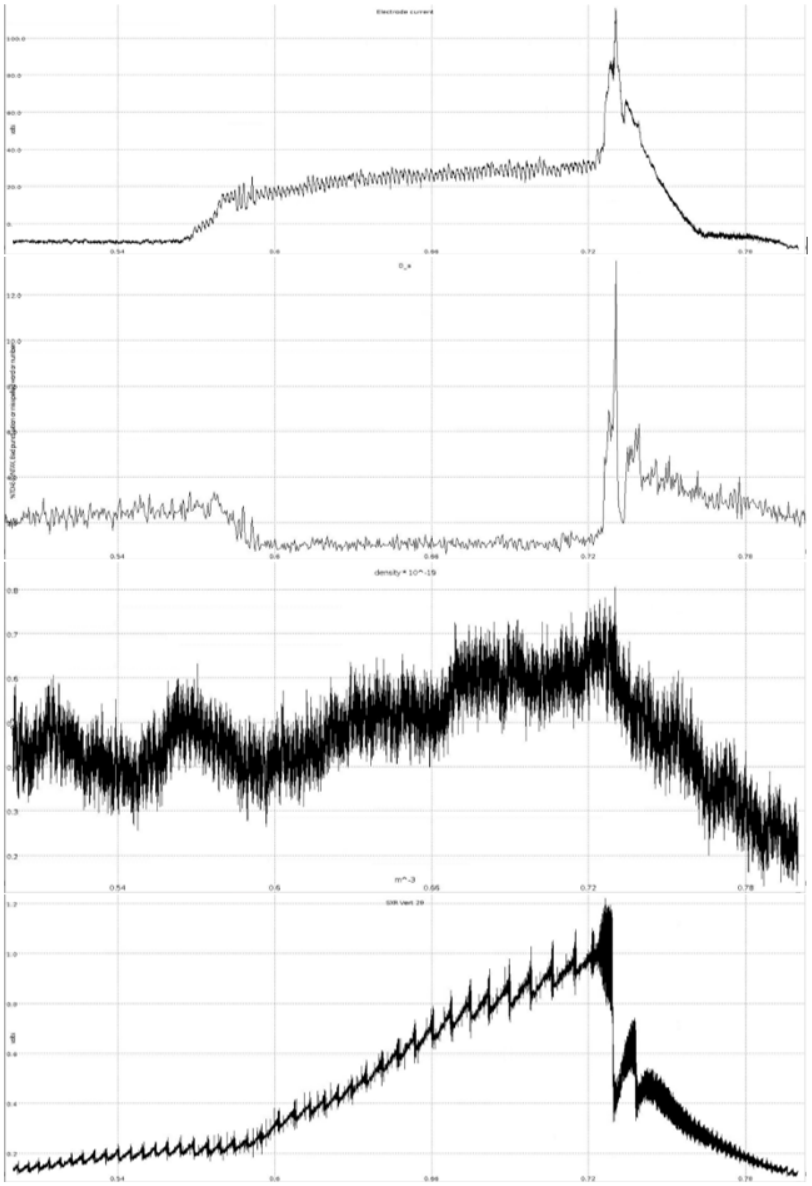

FIGURE 3.7: Are presented in order: the electrode current, the D_α signal, the central line n_e density and the vertical SXR signal. Acquired directly from data.

Chapter 4

Experimental results

In this thesis we have analysed three different discharges, #39136, #39140 and #39143, all of them in Upper Single Null configuration with applied edge biasing: they all exhibit similar features with L-H transition, observed drop of D_α and increase of core density and SXR radiation.
We will report results from shot #39140, since the three analysed discharges were generally reproducible.
The errors of all physical quantities are illustrated in each section.
All the discharges have been analysed distinguishing temporal intervals before and after the L-H transitions. Hence a coherent presentation logic in function of time was required: throughout the thesis the blue and orange colours have been used respectively to indicate conditions in L-mode and H-mode time intervals.

4.1 Characterisation of H-Mode

This section is devoted to the investigation of the effects induced by the L-H transition in the edge profiles, as measured by the U-probe already presented. We will investigate in particular the profile of ion saturation current, as a proxy for the density, of the plasma potential and of the temperature.

4.1.1 Saturation current

The figure 4.1 shows the ion saturation current density profile in function of the distance from the separatrix for the L-Mode and the H-Mode.
The current density signal represents the variation of density through the L-H transition as expressed in equation (3.1). Temperature profile is reported in figure 4.2. Signals used to obtain the temperature has been filtered with a 1 kHz low-pass filter to achieve the averaged values. The temperature values for distances from the separatrix over 0.01m has been considered fixed in the analysis as $8eV \pm 2eV$ because the triple-method measurement often tends to overestimate the temperature near the SOL due to the locally non-Maxwellian distribution of electrons [29].
The errors on distances from the LCFS have been computed as standard deviation

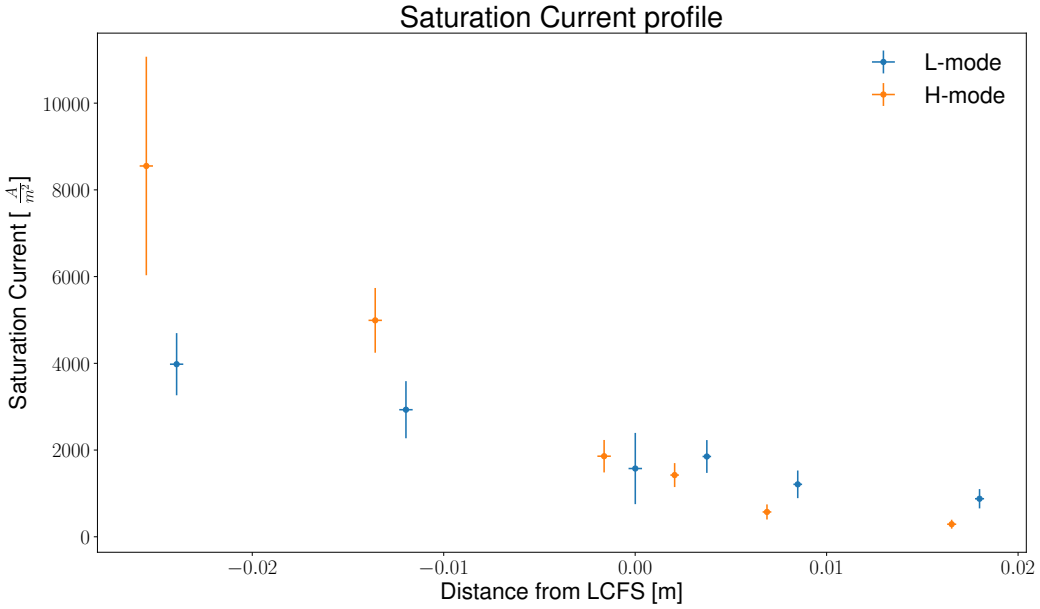

FIGURE 4.1: Saturation current density signal of #39140 from L-Mode to H-Mode.

on the equilibrium values in considered time intervals where the equilibriums instant are evaluated from the specific algorithm as solutions of Grad-Shafranov flux functions of magnetic field contours. The errors on current signal have been computed as standard deviation on all values of the time interval considered. They are evidently different in correspondence of different distances from LCFS. It is probably due to the electronics of each independent tip of the U-probe subject to different turbulence intensities. A variation in the radial derivative of the profile during the H-Mode can be seen and it represents an increase in the density gradient through the transition to the more confined regime. These variations prove the formation of transport barriers.

4.1.2 Plasma potential

The plasma potential is computed indirectly from the measurement of floating potential and temperature of the Langmuir probe:

$$V_p = V_f + \alpha T_e,$$

where V_f is the floating potential and T_e is the electronic temperature. α is a constant which depends only on the type of gas used and is equal to 2.7 for deuterium.
The plasma potential radial profile is reported in figure 4.3 for all temporal intervals during the transition. A spline of 5^{th} order is done useful for subsequent analysis (chapter 4.2).

The errors on floating potential has been taken as standard deviation over the time intervals, as done for saturation current signal. The same for temperature.

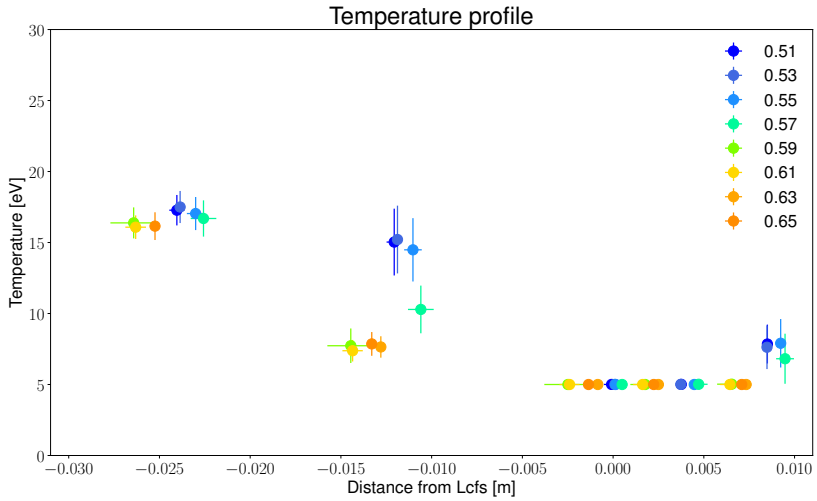

FIGURE 4.2: Temperature signal of #39140 from L-Mode to H-Mode. The L-Mode is before 0.55s. The H-Mode is after 0.61s.

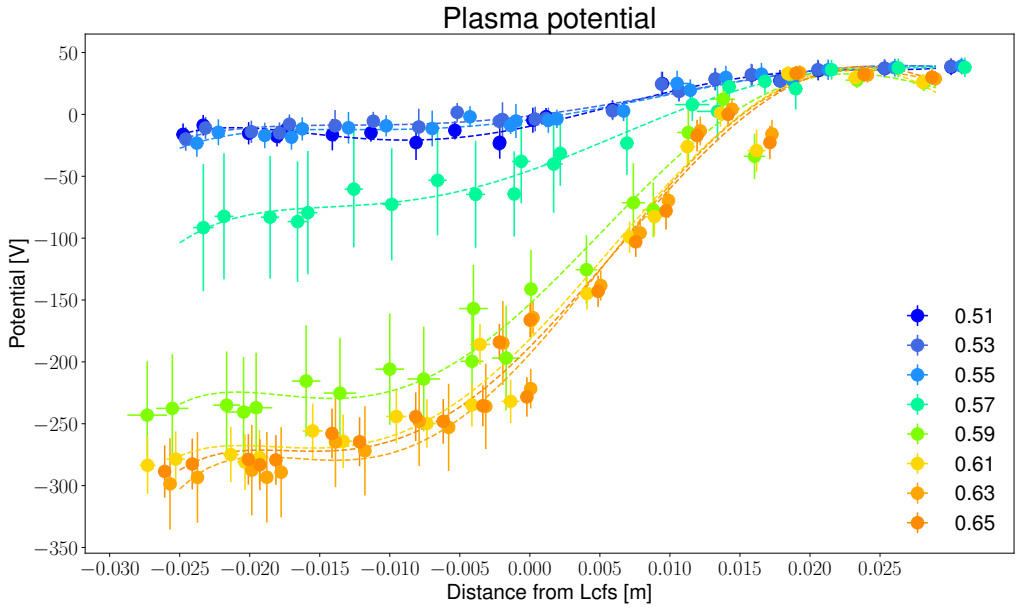

FIGURE 4.3: Plasma potential for different time intervals of #39140 during all the transition from L-Mode to H-Mode. The L-Mode is before 0.55s. The H-Mode is after 0.61s.

The errors on the plasma potential come from the propagation of errors obtained for floating potential and temperature, while α is an error free value.
Clear differences may be observed between the profiles in L and H mode, in particular in the region $-0.01 < R - R_{LCFS} < 0.02$ where stronger gradients are developed, giving rise to a modification of the radial electric field. It leads to change in $E \times B$ velocity and its shear which is related to the second radial derivative of the potential signal.
It can be noticed for 0.57 s and 0.59 s that the signal presents a lot of error mostly due to the fact that these time intervals represents the L-H transition during the change of confinement regime.

4.1.3 Turbulent autocorrelation time

The autocorrelation time represent a characteristic time for describing the intensity of the correlation of a signal with itself in time evolution. Since it is associated with the observed level of turbulence, it is expected to reduce during the L-H transition.
The *Autocorrelation Time* defines the characteristic time τ_{AC} for which a quantity is correlated with itself and it can be expressed as the time such that

$$< f(t)f(t + \tau_{AC}) >= \frac{1}{e} < (f(t))^2 >,$$

where f is the considered physical quantity.
The computation with the factor $\frac{1}{e}$ is totally arbitrary, it can be done also with the factor $\frac{1}{2}$, as it has been done for this analysis, depending on the convention. It just represents a factor to determine the decreasing of the autocorrelation.
It has been obtained directly from saturation current signal and floating potential signals using directly raw signals less subject to error and not derived physical quantities as plasma potential. In order to avoid spurious effects due to the low frequency evolution of the floating potential, which could be disturbed by MHD modes for example, we applied an high pass filtering at 10 kHz, since we are only interested in the turbulence contribution to the signal.
In figure 4.4 the autocorrelation time around the separatrix is reported in function of time during all the transition. It can be seen, for both floating potential and saturation density current, that is reduced for the H-Mode. It has been computed for the same distance from separatrix for current and potential. The errors on time intervals are taken as uniform distribution along the interval hence $\sigma_t = 0.29 \cdot 0.02s = 5.8ms$.
In case of saturation current density signal the autocorrelation time is smaller than the potential one and a greater decrease after the transition can be noticed. It occurs because turbulences are peaks in density and dipoles in potentials hence autocorrelation time of ion saturation current signal which is related to density is reduced more.

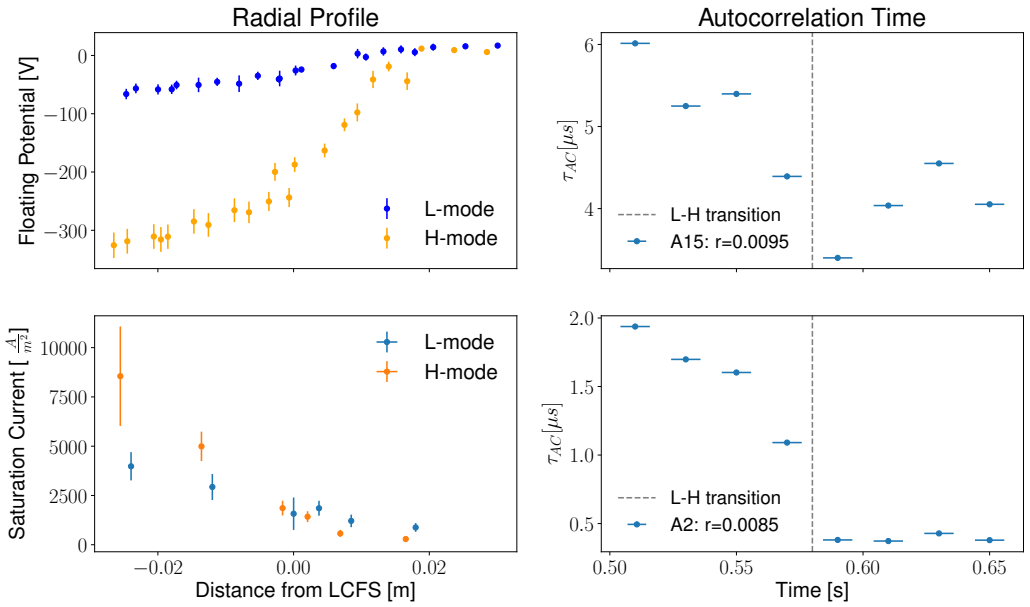

FIGURE 4.4: Floating potential signal and saturation current density autocorrelation time in function of time from L-Mode to H-Mode.

4.2 Zonal Flow study

4.2.1 Flow velocity

The $E \times B$ velocity is given from $\mathbf{v}_{E\times B} = \frac{\mathbf{E}\times\mathbf{B}}{B^2}$. Therefore, considering the dominance of the toroidal component of the magnetic field with respect to the poloidal one, the physical quantity of flow velocity has been computed as follows:

$$v_{E\times B,\theta} \equiv v_\theta = \frac{E_r}{B} = \frac{1}{B}\left(-\frac{\partial}{\partial r}V_p\right), \tag{4.1}$$

where V_p is the plasma potential, B is the radially decreasing magnetic field computed in function of the distance from the centre of tokamak, r is the direction orthogonal to the separatrix.The component along the radial direction is:

$$v_{E\times B,r} \equiv v_r = \frac{E_\theta}{B} = \frac{1}{B}\left(-\frac{\partial}{\partial \theta}V_p\right). \tag{4.2}$$

The values of $E \times B$ velocity has been obtained thanks to the spline of the plasma potential signal, that turned out to be fruitful because the distances from a distinct profile of $V_{E\times B}$ data points would not allowed to obtain a trend as this continuous function provided. In figure 4.5 the $E \times B$ velocity data as direct computation are reported together with the $V_{E\times B}$ function useful for the analysis. The velocity for the case of L-Mode , H-Mode and two time intervals across the transition are reported.
It can be noticed that $V_{E\times B}$ reaches values of 30 $\frac{km}{s}$ during the H-Mode which

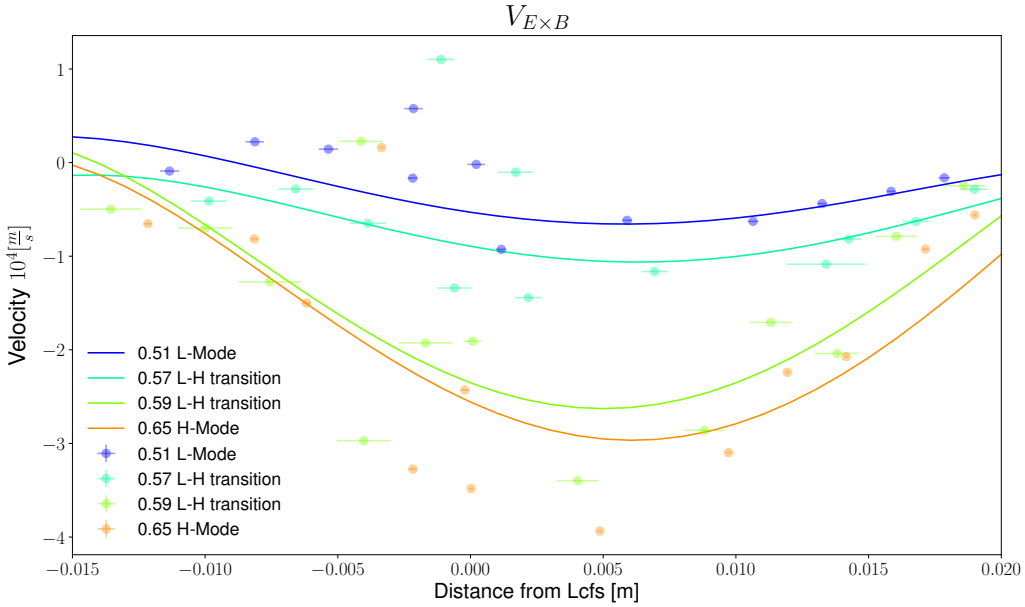

FIGURE 4.5: $E \times B$ velocity for L-Mode, H-Mode and during the transition.

is about 5 times of the L-Mode case. It is noticeable that it is of negative sign which confirms that the acceleration due to the forces which act on the flow are in electron diamagnetic direction as reported in many articles as [18, 19].
Another relevant aspect is that there is not a continuous transition during the L-H transition as can be seen from 0.57 s and 0.59 s cases, when the transition occurs a bit before than 0.58 s. The values double in just 20 ms and this robust and abrupt changes is also seen on the corresponding shear of the $E \times B$ velocity.

4.2.2 Shear

The shear of $E \times B$ velocity is an important physical quantity to consider in the analysis of effects of the L-H transition. Its increase across the transition suggests a variation in the $E \times B$ velocity profile as noticeable also from equations (1.8) and (2.2). The shear is expressed by the radial derivative of the V_{ZF} and it has been obtained from the derivative in function of the distance from the separatrix of the continuous function of $E \times B$ velocity.
It is reported for the intervals of L-Mode and H-Mode and in the middle of the transition (figure 4.6).

The shear assume values of $10^5 - 10^6\, s^{-1}$ coherently with results obtained for many experiments [19, 22–24] and changes from about -3 to $-20 \cdot 10^6 s^{-1}$ in 0.02 s across the transition. Its robust change suggests that the shear can be a relevant quantity in the phenomena of Zonal Flow. This aspect will be taken into account later in the analysis of time evolution of flow acceleration (section 4.2.5).
It can be seen that the shear presents different sign for inner or outer region with

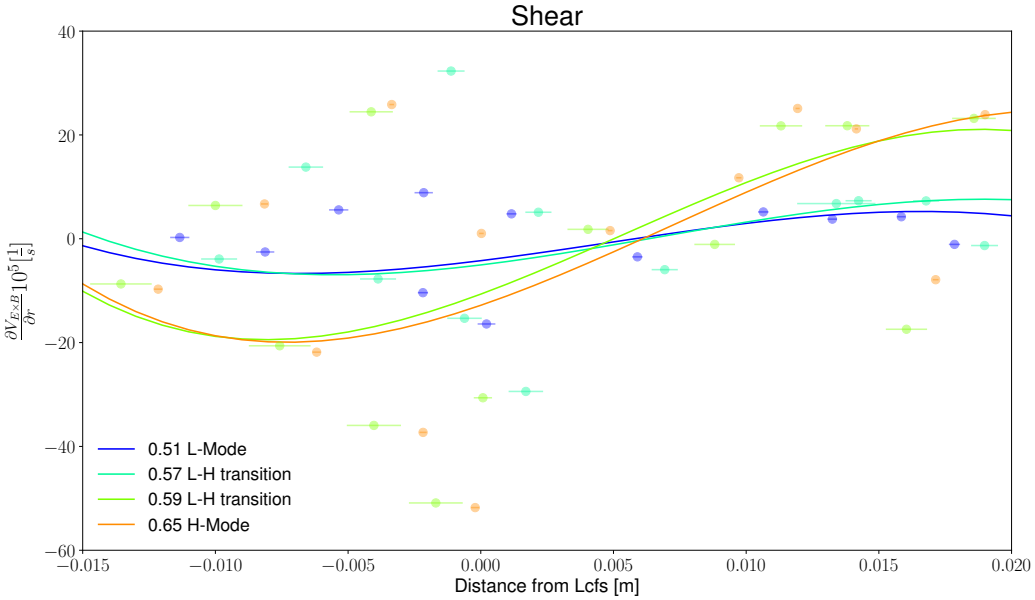

FIGURE 4.6: $E \times B$ shear for L-Mode, H-Mode and during the transition.

respect to the separatrix. These regions in literature are named *Inner Shear Layer* and *Outer Shear Layer* [22]. The presence of this regions also for the L-Mode could be associated to a weak preset phenomenon which tends to displace turbulences towards the edge of the plasma referable to the mean shear flow reported in some experiments [9, 22] interpretable as a self-organising behaviour of the plasma itself. However in the L-Mode is not enough for a confined regime and the action of an external agent as the electric field is required to initiate the phenomenon. The shear intensity is increased for the H-Mode and can be noticed also looking at the variation along the radial direction of $V_{E\times B}$ of figure 4.5, where the velocity tends to return to 0 moving away from LCFS. Therefore this permits to claim that the region of higher shear modification occurs around the separatrix.

4.2.3 Reynolds stress

The fluctuations of the velocity along the poloidal and radial direction has been computed. They correspond to variation in time with respect to their averages of the quantities v_θ and v_r, equations (4.1) and (4.2) respectively.
The computation of the Reynolds stress requires the determination of the fluctuating values of the radial and binormal components velocity. The arrangement of the probe does not allow for a proper determination of these quantities since the Cartesian frame of reference is not aligned with the flux surfaces. Thus we needed to interpolate these quantities in an appropriate frame of references with direction perpendicular and parallel to the local magnetic surface provided by the LCFS. Furthermore this permitted to compute the quantities in function of the distance from the separatrix. In order to maximise the radial resolution, and

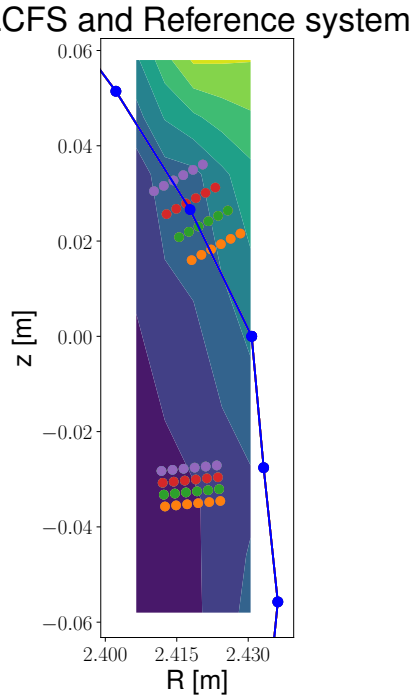

FIGURE 4.7: Rotated reference frame for the analysis of $< \widetilde{v_r}\widetilde{v_\theta} >$ and $< (\widetilde{v_r})^2 >$. The blue points represent the separatrix. The upper and lower grid system are reported.

given the location of the measurements we duplicate the grids in two different z positions as seen in figure 4.7. For each grid the poloidal and radial components has been calculated with derivatives along the points in figure eventually evaluated on central row (represented in red). This procedure allow to exclude the values near the border of measurement system more subject to error in the derivative computation. Due to the necessity of having some grid points across the LCFS it has not been possible to obtain a set of points with radii farther than 0.01m.

Thanks to this system has been possible to estimate the values of the Reynolds Stress $< \widetilde{v_r}\widetilde{v_\theta} >$ as time average of the product of fluctuating parts of $E \times B$ velocity along the two directions. It has been computed also the quadratic fluctuation of the radial component $< (\widetilde{v_r})^2 >$, useful to a secondary analysis reported in section 4.3. These quantities can be seen in figure 4.8.

In this section the distances from separatrix are taken as ideal because they are obtained in function of rotated frame starting from original R and Z positions of the U-probe tips that are fixed and preset as error free. The errors on the fluctuations are computed as standard deviation on each time interval considered of the final computed quantity. It can be seen that errors are considerable for the quantities computed during the L-H transition due to the strong intensity of the fluctuations being subject to the external agent that led to the variation of the confinement regime.

The fluctuations reach values up to $10^6 \frac{m^2}{s^2}$. It can be seen, for both $< (\widetilde{v_r})^2 >$

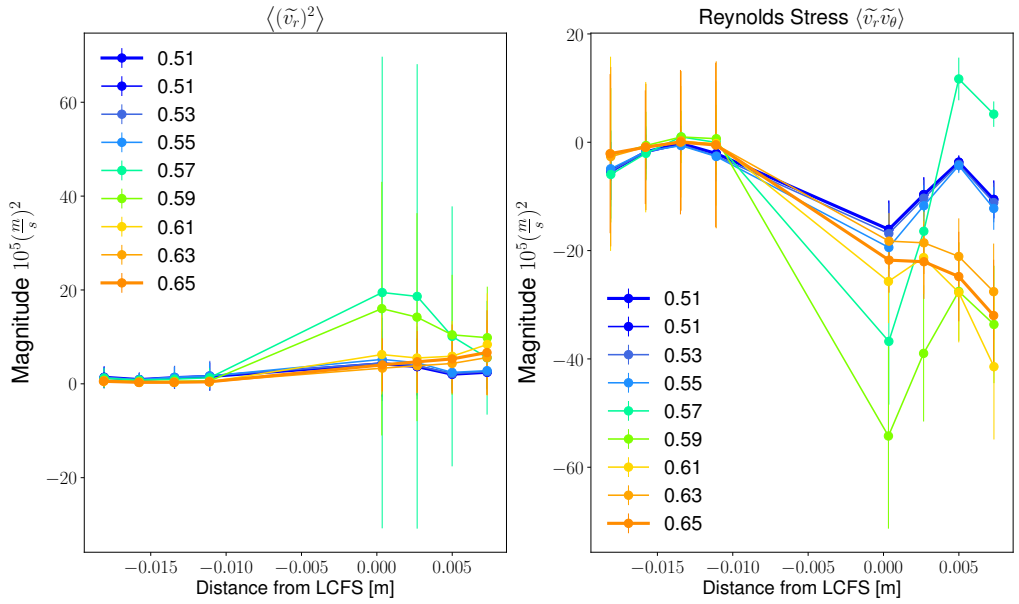

FIGURE 4.8: Averages of floating potential fluctuations of product quantities of v_θ and v_r. For each plot the lines for the first time interval of the L-Mode and the last one of the H-Mode are plotted wider than other time intervals.

and Reynolds stress, that the quantities during the L-H transition (about 0.578s) has magnitude at least double the most value assumed before and after the transition. It can be interpreted as the absorption of energy from the external phenomena which initiates the transition. This energy will be then transferred to the Zonal Flow through the force which acts thanks to the radial derivative of the Reynolds stress. It performs a change of regime with an increase in velocity of about $2 \cdot 10^4 \frac{m}{s}$ in 0.02 s. A robust change from flat plasma potential to a sheared one in the same time can be noticed.
One might think that this behaviour for L-H transition could be due to a last attempt of a re-organising process of plasma just before the system completely change towards the confined regime, as reported in section 2.2.3 for many experiments in case of LCOs [9, 22]. Nevertheless this phenomenon does not happens here due to the method with which the transition has been triggered: the external electric field. The absence of LCOs is verified in next section. The importance of the exploitation of electric field in the dynamics of the phenomenon will be better treated in section 4.2.5.

4.2.4 Shearing rate and Turbulent rate

When the H-Mode transition occurs the shearing rate exceed the turbulent rate. This is a manifestation of turbulences reduction where the shear intensity increases more than the increase of turbulent decorrelation rate and this represents

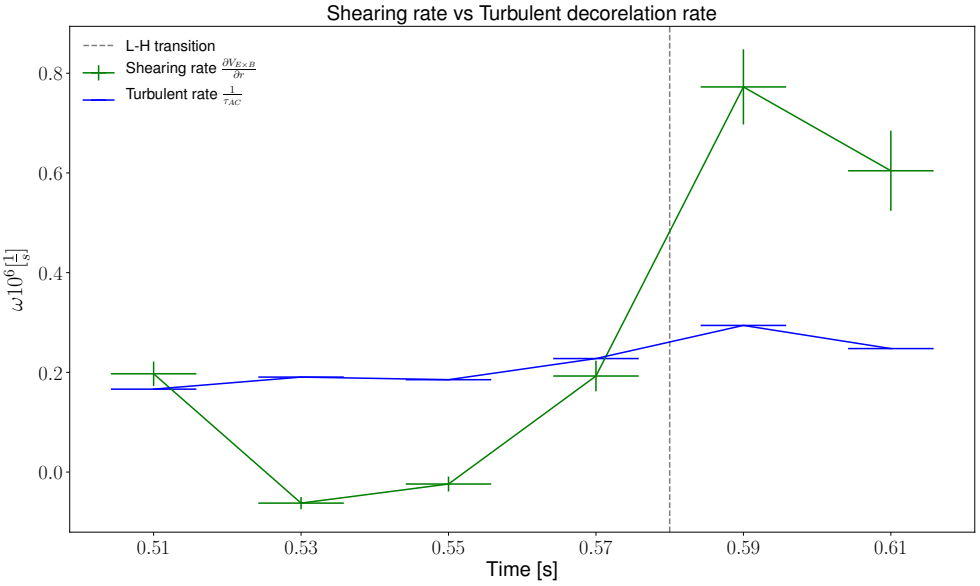

FIGURE 4.9: Shearing rate and turbulent decorrelation rate across the transition.

the changing to the more confined regime, as described in section (2.2.1). Comparing the time evolution of shearing rate against the turbulent decorrelation rate has been verified that the former exceed the latter as expected since the transition to the H-Mode occurs, as verified from previous physical quantities.
It has been analysed this trend in function of time for the radial position just outside the separatrix at $R - R_{LCFS} = 0.009m$. It is reported in figure 4.9.
The turbulent rate has been estimated as the inverse of the autocorrelation time of section 4.1.3. The error-bars on the shearing rate are taken as standard deviations of the values around the radial position corresponding to the computed autocorrelation time, this for each time interval.
Looking at the behaviour of turbulent rate in function of time it increases from $2 \cdot 10^5\ s^{-1}$ to $3 \cdot 10^5\ s^{-1}$ but the shearing rate increases of a significant extent to exceed the value of turbulent rate confirming the confined regime of the H-Mode.
Having analysed the physical quantities for all the time interval, not only around the L-H transition, is evident that the system does not exhibit Limit Cycle Oscillations for the case of induced H-Mode from a biased electrode.

4.2.5 Analysis of Zonal Flow model for biased induced H-Mode

In this section are reported the results of the analysis of the flow acceleration along poloidal direction compared to the intensity of the Reynolds Stress force expressed as $-\frac{\partial}{\partial r}\langle \widetilde{v_r}\widetilde{v_\theta}\rangle$.
This is based on the analysis of the Zonal Flow model reported in section 2.2.1 and on momentum balance equation (1.8). As can be seen from the analysis of $V_{E\times B}$ (figure 4.5) from 0.59 s to 0.65 s the system undergoes an acceleration of

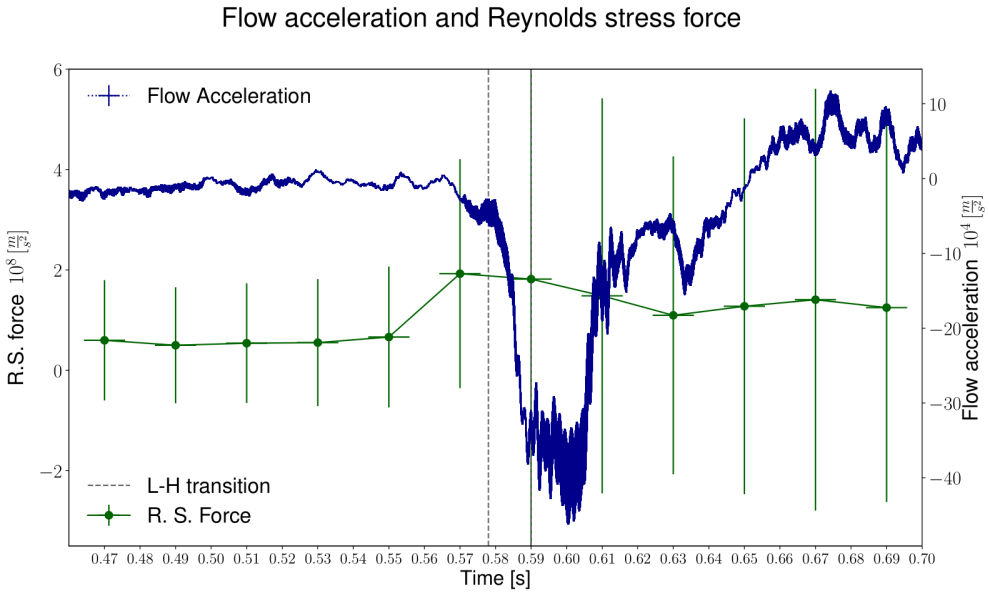

FIGURE 4.10: Reynolds stress force and flow acceleration are reported. They are respectively in scale of $10^8 \frac{m}{s^2}$ and $10^4 \frac{m}{s^2}$.

$\simeq 10^4 - 10^5\ m/s^2$ for -0.005 m $< R - R_{LCFS} <$ 0 m. While looking at the results obtained for the Reynolds stress (figure 4.8) in the same spatial range the radial derivative seems of the order of $\simeq 10^7 - 10^8\ m/s^2$. Hence is evident that in the momentum balance there are huge damping terms to consider. Furthermore the Reynolds stress manifests an abrupt increasing in the intensity for the time interval during the L-H transition but the phenomena of LCOs is not manifested, as appeared from the turbulent rate analysis in previous section, hence other self-organising mechanisms of the plasma are present.
Therefore the hypothesis of a forcing quantity due to the ignition of the electrode has to be analysed.

The time derivative of $E \times B$ velocity and the opposite of radial derivative of Reynolds stress for the same spatial range are reported. It has been analysed for $-0.005\,m < R - R_{LCFS} < 0\,m$ which is a region just inside the separatrix of interest for the characteristics of the H-Mode. It corresponds to a radial position of decreasing $V_{E\times B}$.
This analysis has been done considering a time interval starting prior to time intervals considered for previous sections. The comparison starts at 0.45 s when the electrode had not still been ignited and the difference in intensities between the ZF acceleration and RS force can be seen in figure 4.10. Is peculiar what occurs during the L-H transition.
To obtain the errors on the time derivative of the flow velocity an error on the average on the spatial range has been taken for each instant. The error on the Reynolds stress force has been obtained as propagation on the errors on Reynolds

stress in the considered range as a discrete derivative for each time interval of previous analysis (section 4.2.3).
The ZF acceleration during the L-Mode is of the order of $\simeq 4 \cdot 10^4\, m/s^2$ or a little less, as expected from a rough estimation from figure 4.5. Is evident that after the transition to the H-Mode the flow acceleration comes back towards positive values. It occurs when the RS force decreases. Hence there exists a mechanism opposite to $-\frac{\partial(RS)}{\partial r}$ that contributes to the V_{ZF}. This could be related to a quantity that drives against the RS force towards the original equilibrium. Furthermore looking at the L-Mode the flow acceleration is almost 0 and the RS force of about $1 \cdot 10^8\, m/s^2$ hence a difference of the order of magnitude of $10^8\, m/s^2$ is present and has to be associated to a damping mechanism. The acceleration produced from the Reynolds stress is of the order of $10^8\, m/s^2$ hence having a flow velocity of $10^4\, m/s$ it would imply a damping coefficient of $10^3 - 10^4\, 1/s$ which results small compared to the turbulent rate of $10^5\, 1/s$ (figure 4.9). Furthermore from a simple computation of the difference between the intensity of the flow acceleration and the Reynolds stress force it results that it is not linearly dependent in velocity as for the original Zonal Flow model and the dependence on velocity changes a lot in function of which time condition is taken. Therefore additional terms has to be considered in case of induced H-Mode. One of them is probably proportional to the electric field which triggers the transition. Another one is suggested directly looking at the balance momentum equation (1.8) where the Laplacian of the velocity expressed in cylindrical coordinates contains terms proportional to the shear and its radial derivative. These terms are extremely difficult to estimate experimentally due to the associated error from the propagation of related physical quantities. A starting improved model has to be implemented. This is beyond the scope of this thesis but it is a suggestion for future works.

Observing the peak of the Reynolds stress it occurs before the transition and compared to $E \times B$ flow increase can be noticed that this latter occurs in late with respect to Reynolds stress increase. Furthermore the Reynolds stress magnitude is reduced after the transition. With these observations seems that the $E \times B$ velocity assumes one value during the L-Mode and it increases (as in figure 4.5) thanks to the Reynolds stress, but this latter is not enough to lead to the confined regime unless an external agent acts on the system. Hence this external force results in the enhancement of the phenomena which increases the $E \times B$ velocity and consequently the turbulences reduction.
Therefore the evidences that the Reynolds stress force decreases before the L-H transition and the flow acceleration starts to increase (towards negative values) when the Reynolds stress force starts to decrease in intensity are proofs that the Reynolds stress force acts as intermediary gaining energy from the external agent and then transferring it to the flow increasing its velocity and eventually reducing turbulences.

4.3 Additional analysis: anomalous transport

In this section a further analysis is reported with the aim to estimate the turbulent contribute to viscosity in the anomalous transport. A method to obtain this quantity has been recently proposed in the article of T.Long et al. on the HL-2A tokamak [23] where the Reynolds tensor is decomposed in different stresses. It allows to obtain a contribute in the Reynolds stress $\langle \widetilde{v_r}\widetilde{v_\theta}\rangle$ directly depending on the shear. In this way a diffusive transport due to turbulences can be deduced. The expression of the Reynolds stress is the following:

$$\langle \widetilde{v_r}\widetilde{v_\theta}\rangle = -\chi_\theta \frac{\partial v_\theta}{\partial r} + v_r^{eff} < v_\theta > + \Gamma_{r\theta}^{Res},$$

where $-\chi_\theta \frac{\partial v_\theta}{\partial r}$ is the diffusive stress due to turbulent momentum diffusion, with χ_θ the turbulent viscosity for the flow. $v_r^{eff} < v_\theta >$ is the radial convection of poloidal momentum and compared to the viscous diffusion it can be neglected in the strong shear layer at the edge of the plasma. The last term on R.H.S. is the residual stress which does not depend on the flow velocity or its shear but it is a function of temperature and density profiles. This latter contribute has not been completely analysed in this thesis but it is suggestion fo further analysis.
The analysis done on HL-2A tokamak has been performed only for L-Mode discharges with ohmic heating or electron cyclotron resonance heating (ECRH). Therefore an eventual exceeding of power threshold to obtain the H-Mode would have damaged the measurement system. Here, being the H-Mode obtained through induced electric field, the implementation for the H-Mode has been possible.

4.3.1 Turbulent contribution to viscosity

Therefore the turbulent viscosity contribution has been analysed:

$$\chi_\theta = < (\widetilde{v_r})^2 > \tau_{AC}$$

where τ_{AC} is the turbulent autocorrelation time and $\frac{\partial v_\theta}{\partial r}$ obviously the $E \times B$ shear. $< (\widetilde{v_r})^2 >$ has been obtained with the same frame used for Reynolds Stress. It is reported in figure 4.8.
To obtain the values of the coefficient has been done splines on τ_{AC} and then evaluated in the points in which $< (\widetilde{v_r})^2 >$ has been obtained. Finally the product in the L-Mode and the H-Mode has been computed. These are reported in figure 4.11.

The values of the turbulent contribute to the viscosity in the L-Mode has been found to be smaller than $2\, m^2/s$ as for T.Long et al. experiment and this contribute is almost uniform with a little increase before the separatrix. The results obtained here for the H-Mode show instead a contribute to the anomalous transport throughout increasing radii. It represents a radial region towards which turbulences are moved and confined, hence the transport due to them increases.

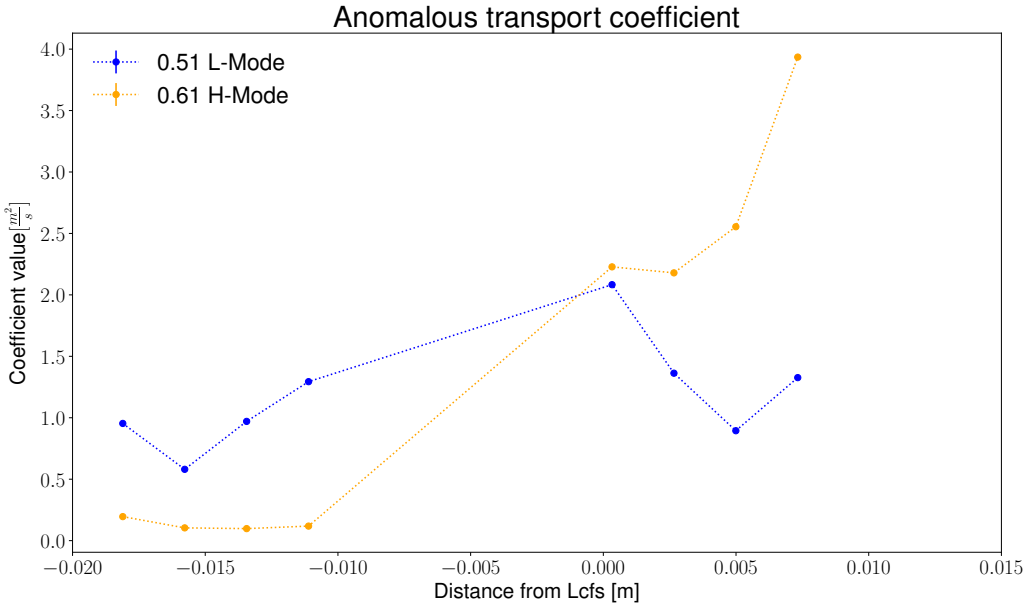

FIGURE 4.11: Turbulent viscosity for L-Mode and H-Mode.

4.3.2 Turbulent diffusive stress

Once estimated the turbulent viscosity the computation of the diffusive stress has been possible evaluating the shear $\frac{\partial v_\theta}{\partial r}$ in the same radial positions of the viscosity coefficient. It is reported in figure 4.12.

The diffusive stress $\Gamma_{Diff} = -\chi_\theta \frac{\partial v_\theta}{\partial r}$ can be interpreted as a diffusive momentum transfer as if we analysed the momentum balance equation from a diffusive point of view. Hence the area where this quantity turns out to be greater defines the zone towards which the momentum transfer is stronger. The negative values would represent a momentum transfer in opposite radial direction.

In the case of L-Mode the same order of magnitude and trend reported in the T.Long et al. article for negative radii with respect to the separatrix can be seen. Furthermore with this analysis this quantity results stronger in the same region of the viscosity coefficient. In that region the contribute of the shear during the L-Mode can be seen to be present but not so robust (figure 4.6).

For the H-Mode an increase in the turbulent diffusive stress for the radial area around the separatrix can be seen. It is coherent with the region of most increasing Reynolds stress (figure 4.8) and the $E \times B$ velocity from instants during L-H transition to H-Mode (figure 4.5).

Hence the confinement region around the separatrix is confirmed, consistently with results obtained in the rest of thesis.

A rough estimation of the order of magnitude of residual stress can be done. Looking at the values of Reynolds stress and diffusive stress for the same time intervals, that in this analysis defines the L-Mode and the H-Mode, an order of magnitude can be estimated. For the L-Mode the residual stress results of the order of $-2 \cdot 10^6 \frac{m^2}{s^2}$ greater than HL-2A tokamak, due to greater Reynolds stress. For the

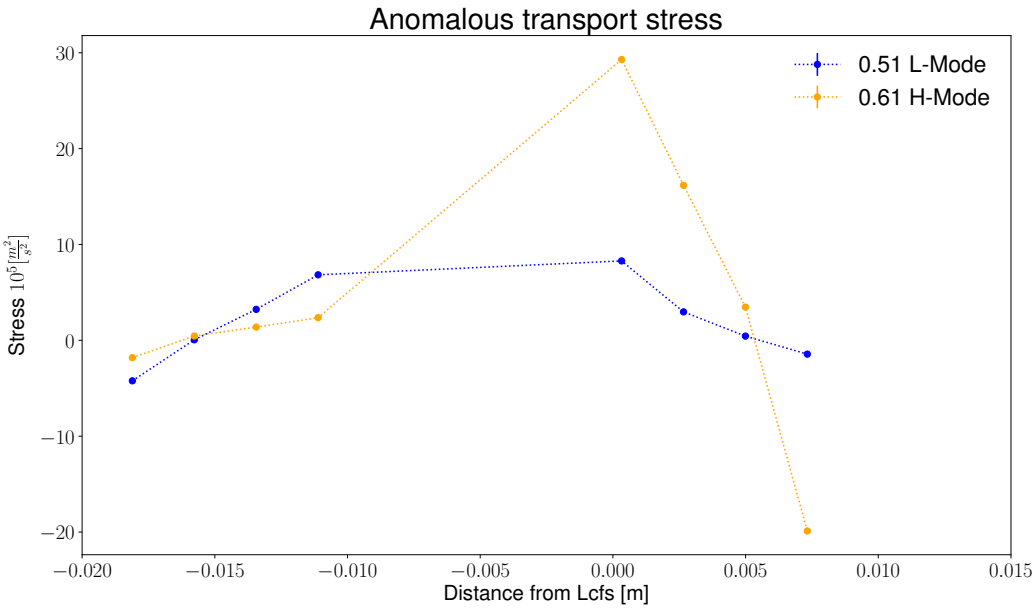

FIGURE 4.12: Turbulent diffusive stress for L-Mode and H-Mode.

H-Mode it reaches values up to $-5 \cdot 10^6 \frac{m^2}{s^2}$ at the position of $R - R_{LCFS} = 0$.

Chapter 5

Conclusions

Through the work of this thesis the dynamics of self-organising processes of plasma has been studied. The importance of the Reynolds stress in the attainment of a regime of turbulences reduction has been confirmed. The transition to the High confinement Mode has been achieved through the exploitation of an external electrode. The method of harnessing an electric field to induce the H-Mode is again validated through the physical quantities analysed that testify the occurrence of this more confined regime. A robust increase in the velocity and its shear have been verified. Values of $30\,km/s$ are found to be reached from the flow velocity during the transition and of $2 \cdot 10^6\,s^{-1}$ for the shear. This demonstrate a change in the regime for which the turbulent eddies are stretched and thus destroyed. During the transition from L to H mode other modifications of plasma profile are observed as well, as the steepening of the density gradient, the variation of the momentum turbulent diffusion and the contribution to momentum generation by the Reynolds stress mechanism, which has been the subject of the present thesis.
In this induced transition to the H-Mode the LCOs have not manifested.
A remarkable aspect is that all these physical quantities have been verified for all the analysed discharges and they have similar or identical behaviour demonstrating the reproducibility of the studied phenomena.

A fundamental result of the analysis done during the work of this thesis is the evidence that the Reynolds stress acts as intermediary to transfer the energy from the external electric field to the plasma resulting in an increase of the flow velocity and hence turbulences reduction. An increase in the Reynolds stress before the L-H transition is manifested and the delay between the increase of the flow acceleration and the decrease of the force generated from the Reynolds stress testify the relevant role of the Reynolds stress in the achievement of the H-Mode. The external agent which initiate the process of Reynolds stress force reinforcement is associated to the external electric field induced from the electrode. The role of energy transfer of the force acted from Reynolds stress can explain also the strong variation of the Reynolds stress found during the L-H transition (figure 4.8), with values completely different from the ones in the L-Mode and the H-Mode. These

time intervals represent the instants in which the RS absorbs energy from the external agent and then transfers it to the flow. Coherently the flow velocity (figure 4.5) does not manifest this behaviour, because it is the target of the energy transfer and does not undergo intermediate actions.

An analysis of the Zonal Flow model for the case of induced biased H-Mode, as for discharges analysed in this work, reported that other forces have to be considered to have a complete model. Some theoretical hypothesis of possible additive terms can be done. Significant terms can be obtained for the equation (2.1) considering contributes of non turbulent nature from the momentum balance equation (1.8). A complete analysis allows to achieve the order of magnitude of radial electric field and furthermore the flow damping ν_d. From a first sight at the MHD equations (1.6) and (1.5) inserted in the momentum balance equation (1.8) the contribute of the electric field created from the external electrode can be obtained. Considering $\mathbf{E}$ radially directed and $\mathbf{v} \times \mathbf{B}$ from Ohm's law radially inward directed, one term results, contributing to the increase of flow acceleration intensity. This term is related to the induced electric field as $\frac{\sigma B}{\rho} E$, where the conductivity σ can be found thanks to Spitzer resistivity and ρ from saturation current density signal. Besides the electric field contribute also a thorough analysis on the force which acts against the Reynolds stress force should be done to obtain a complete model. This has been suggested to be related to the shear through the Laplacian of the flow velocity, which is neglected in the previous model, but here has to be evaluated taking into account the multiplying factor, which is the viscosity, that has been proved to increase a lot for the induced H-Mode. Taking into accounts all this for different radii and considering all the possible contributions to an implementation of a new Zonal Flow model for biased induced H-Mode is suggested for future analysis.
In addition further analysis are proposed. In the computation of the Reynolds stress has not been possible to obtain informations for distances from the separatrix greater than 0.008m and possible interesting analysis can be done investigating deeper in the SOL the force acted from the Reynolds stress compared with other forces. Furthermore an interesting topic just mentioned in the thesis (section 2.1) and not treated due to the required time for this type of analysis, is the study of hysteresis-like behaviour manifested in some RFX-mod discharges in the same biased induced H-Mode configuration [21]. The idea is that analysing which physical quantities maintain the effects of the H transition, after having turned off the electrode, could reveal the real nature of the H-Mode.

In conclusion the Reynolds stress has seen to have a fundamental role in turbulences reduction and self-organising mechanisms of plasma. Nonetheless it is not the only force at work. Is evident that the induced electric field and the shear play an important role in this mechanism. Thanks to the results obtained during this thesis, in comparison with theory and model at present existent, suggestions

for future analysis are proposed to be done for a complete understanding of the phenomenon of transition to the High confinement Mode obtained through edge biasing technique.

Acknowledgements

I did my thesis work at Consorzio RFX in CNR of Padova. I would like to thank my co-supervisor Dr. Nicola Vianello for the kind helpfulness and expertise in the realization of this thesis. Moreover I would like to thank my supervisor and all the RFX group for the welcoming and pleasant working environment.
I would like to thank Università degli Studi di Padova for the possibility to collaborate with RFX on this thesis project.
Last but not least I thank all my friends and relatives that supported me
and shared with me these relevant years making this essential path of my life pleasant.

List of Abbreviations

MHD	**M**agneto**H**ydro**D**ynamics
SOL	**S**crape **O**ff **L**ayer
L-Mode	**L**ow (confinement) **M**ode
H-Mode	**H**igh (confinement) **M**ode
RS	**R**eynolds **S**tress
ZF	**Z**onal **F**low
LCFS	**L**ast **C**lose **F**lux **S**urface

Physical Constants

Boltzmann Constant	$k_B = 8.617\,333\,262 \times 10^{-5}\,\mathrm{eV\,K^{-1}}$	$1.380\,649 \times 10^{-23}\,\mathrm{J\,K^{-1}}$ (exact)
Elementary Charge	$e = 1.602\,176\,634 \times 10^{-19}\,\mathrm{C}$ (exact)	
Speed of Light	$c = 2.997\,924\,58 \times 10^{8}\,\mathrm{m\,s^{-1}}$ (exact)	
Electron mass	$m_e = 9.109\,383\,701\,5(28) \times 10^{-31}\,\mathrm{kg}$	$0.510\,998\,950\,00(15)\,\mathrm{MeV/c^2}$

Bibliography

[1] Lepine-Szily et al. "Nuclear astrophysics: Nucleosynthesis in the Universe". In: *International Journal of Astrobiology* 11 (Oct. 2012), pp. 243–250. DOI: 10.1017/S1473550412000158.

[2] A.S. Richardson. *2019 NRL Plasma Formulary*. Plasma Physics Division. 2019. URL: https://www.nrl.navy.mil/ppd/content/nrl-plasma-formulary.

[3] D. Testa, M. Cecconello, and C. Schlatter and. "The dependence of the proton–triton thermo-nuclear fusion reaction rate on the temperature and total energy content of the high-energy proton distribution function". In: *Nuclear Fusion* 49.6 (2009), p. 062004. DOI: 10.1088/0029-5515/49/6/062004. URL: https://doi.org/10.1088%2F0029-5515%2F49%2F6%2F062004.

[4] M. Zuin et al. "Overview of the RFX-mod fusion science activity". In: *Nuclear Fusion* 57.10 (2017), p. 102012. DOI: 10.1088/1741-4326/aa61cc. URL: https://doi.org/10.1088%2F1741-4326%2Faa61cc.

[5] Arnab Rai Choudhuri. *The Physics of Fluids and Plasmas: An Introduction for Astrophysicists*. Ed. by Cambridge University Press. 2008.

[6] N Vianello et al. "Turbulence, flow and transport: hints from reversed field pinch". In: *Plasma Physics and Controlled Fusion* 48.4 (2006), S193–S203. DOI: 10.1088/0741-3335/48/4/s14. URL: https://doi.org/10.1088%2F0741-3335%2F48%2F4%2Fs14.

[7] C. Stan-Sion and Alexandru Petre. "AMS measurements of fuel retention on the surface of materials used in fusion experiments". In: *UPB Scientific Bulletin, Series A: Applied Mathematics and Physics* 76 (Jan. 2014), pp. 265–274.

[8] Chen Ming Rao Bo Chen Jie Chen Zhao-Quan Xiao Jin-Shui Hu Xi-Wei Xiong Hao Liu Ming-Hai†. "Radial magnetic field in magnetic confinement device". In: *Chinese Physics B* (2009). URL: http://cpb.iphy.ac.cn/article/2015/cpb_24_9_095202.html.

[9] G R Tynan et al. "Recent progress towards a physics-based understanding of the H-mode transition". In: *Plasma Physics and Controlled Fusion* 58.4 (2016), p. 044003. DOI: 10.1088/0741-3335/58/4/044003. URL: https://doi.org/10.1088%2F0741-3335%2F58%2F4%2F044003.

[10] R D Smirnov et al. "Modelling of dynamics and transport of carbon dust particles in tokamaks". In: *Plasma Physics and Controlled Fusion* 49.4 (2007), pp. 347–371. DOI: 10.1088/0741-3335/49/4/001. URL: https://doi.org/10.1088%2F0741-3335%2F49%2F4%2F001.

[11] B. Chapman et al. “High confinement plasmas in the Madison Symmetric Torus reversed-field pinch”. In: *Physics of Plasmas* 9 (May 2002), pp. 2061–2068. DOI: 10.1063/1.1456930.

[12] B.Sc. Hugh P. Callaghan. “Stellarator equilibrium reconstruction by function parameterization”. Degree of Doctor of Philosophy. National University of Ireland, 1999. URL: http://physics.ucc.ie/pjm/trachtais_macleinn/HughCallaghanPhD1999/thesis_simple.html.

[13] Robert Arnoux. “How Fritz Wagner "discovered" the H-Mode”. In: *ITER Newsline* (2009). URL: https://www.iter.org/newsline/86/659.

[14] L. Laurent. *Improvement of the tokamak concept*. 1994. URL: https://inis.iaea.org/collection/NCLCollectionStore/_Public/28/016/28016718.pdf.

[15] J.A Snipes et al. “H mode power threshold database for ITER”. In: *Nuclear Fusion* 36.9 (1996), pp. 1217–1264. DOI: 10.1088/0029-5515/36/9/i11. URL: https://doi.org/10.1088%2F0029-5515%2F36%2F9%2Fi11.

[16] K. Itoh A. Yoshikawa S.I. Itoh. *Plasma and Fluid Turbulence: Theory and Modelling*. Institue of Physics. Series in Plasma Physics, 2002.

[17] Sergey Soldatov et al. “Turbulence, flows and edge localized mode (ELM) dynamics in limiter H-mode plasmas in TEXTOR”. In: *Plasma Physics and Controlled Fusion* 52 (June 2010), p. 085001. DOI: 10.1088/0741-3335/52/8/085001.

[18] G R Tynan, A Fujisawa, and G McKee. “A review of experimental drift turbulence studies”. In: *Plasma Physics and Controlled Fusion* 51.11 (2009), p. 113001. DOI: 10.1088/0741-3335/51/11/113001. URL: https://doi.org/10.1088%2F0741-3335%2F51%2F11%2F113001.

[19] L. Schmitz. “The role of turbulence–flow interactions in L- to H-mode transition dynamics: recent progress”. In: *Nuclear Fusion* 57.2 (2017), p. 025003. DOI: 10.1088/1741-4326/57/2/025003. URL: https://doi.org/10.1088%2F1741-4326%2F57%2F2%2F025003.

[20] T. Kobayashi et al. “Model validation for radial electric field excitation during L–H transition in JFT-2M tokamak”. In: *Nuclear Fusion* 57.7 (2017), p. 072005. DOI: 10.1088/1741-4326/aa5d03. URL: https://doi.org/10.1088%2F1741-4326%2Faa5d03.

[21] M. Spolaore et al. “H-mode achievement and edge features in RFX-mod tokamak operation”. In: *Nuclear Fusion* 57.11 (2017), p. 116039. DOI: 10.1088/1741-4326/aa7f1e. URL: https://doi.org/10.1088%2F1741-4326%2Faa7f1e.

[22] L. Schmitz et al. “Role of Zonal Flow Predator-Prey Oscillations in Triggering the Transition to H-Mode Confinement”. In: *Phys. Rev. Lett.* 108 (15 2012), p. 155002. DOI: 10.1103/PhysRevLett.108.155002. URL: https://link.aps.org/doi/10.1103/PhysRevLett.108.155002.

[23] T. Long et al. “Studies of Reynolds stress and the turbulent generation of edge poloidal flows on the HL-2A tokamak”. In: *Nuclear Fusion* 59.10 (2019),

p. 106010. DOI: 10.1088/1741-4326/ab33cf. URL: https://doi.org/10.1088%2F1741-4326%2Fab33cf.

[24] Grenfell et al. "Turbulent filament properties in L and H-mode regime in the RFX-mod operating as a tokamak". In: *Internal pubblication of RFX - CNR* (2019).

[25] EFDA Phil Dooley. "A predator-prey relationship in the plasma jungle". In: *ITER Newsline* (2013). URL: https://www.iter.org/newsline/256/1480.

[26] Ondrej Kudlacek. "Real time measurement of plasma macroscopic parameters on RFX-mod using a limited set of sensors". In: *Physics of Plasmas* 22 (Oct. 2015). DOI: 10.1063/1.4932992.

[27] Dr Paul May. *MSc Physics of Advanced Semiconductor Materials, Plasmas and Plasma Processing, Plasma Diagnostics: Electron Temperatures and Ion Energy Distributions*. 1998. URL: http://www.chm.bris.ac.uk/~paulmay/misc/msc/msc4.htm.

[28] Wing Tsui et al. "A new scheme for Langmuir probe measurement of transport and electron temperature fluctuations". In: *Review of Scientific Instruments* 63 (Nov. 1992), pp. 4608 –4610. DOI: 10.1063/1.1143683.

[29] D. Tskhakaya et al. "Interpretation of divertor Langmuir probe measurements during the ELMs at JET". In: *Journal of Nuclear Materials* 415 (Aug. 2011). DOI: https://doi.org/10.1016/j.jnucmat.2010.10.090.